PHENOTYPING OF HYPERTENSIVE HEART DISEASE AND HYPERTROPHIC CARDIOMYOPATHY USING PERSONALIZED 3D MODELING AND CARDIAC MAGNETIC RESONANCE IMAGING

CHUAH SHOON HUI

FACULTY OF ENGINEERING
UNIVERSITY OF MALAYA
KUALA LUMPUR

2020

PHENOTYPING OF HYPERTENSIVE HEART DISEASE AND HYPERTROPHIC CARDIOMYOPATHY USING PERSONALIZED 3D MODELING AND CARDIAC MAGNETIC RESONANCE IMAGING

CHUAH SHOON HUI

DISSERTATION SUBMITTED IN FULFILMENT OF THE REQUIREMENTS FOR THE DEGREE OF MASTER OF ENGINEERING SCIENCE

FACULTY OF ENGINEERING
UNIVERSITY OF MALAYA
KUALA LUMPUR

2020

UNIVERSITY OF MALAYA

ORIGINAL LITERARY WORK DECLARATION

Name of Candidate: Chuah Shoon Hui

Matric No: KGA180021

Name of Degree: Master of Engineering Science

Title of Project Paper/Research Report/Dissertation/Thesis ("this Work"):

Phenotyping of Hypertensive Heart Disease and Hypertrophic Cardiomyopathy using Personalized 3D Modeling and Cardiac Magnetic Resonance Imaging

Field of Study: Biomedical Engineering

I do solemnly and sincerely declare that:

(1) I am the sole author/writer of this Work;
(2) This Work is original;
(3) Any use of any work in which copyright exists was done by way of fair dealing and for permitted purposes and any excerpt or extract from, or reference to or reproduction of any copyright work has been disclosed expressly and sufficiently and the title of the Work and its authorship have been acknowledged in this Work;
(4) I do not have any actual knowledge nor do I ought reasonably to know that the making of this work constitutes an infringement of any copyright work;
(5) I hereby assign all and every rights in the copyright to this Work to the University of Malaya ("UM"), who henceforth shall be owner of the copyright in this Work and that any reproduction or use in any form or by any means whatsoever is prohibited without the written consent of UM having been first had and obtained;
(6) I am fully aware that if in the course of making this Work I have infringed any copyright whether intentionally or otherwise, I may be subject to legal action or any other action as may be determined by UM.

Candidate's Signature Date:

Subscribed and solemnly declared before,

Witness's Signature Date:

Name:

Designation:

PHENOTYPING OF HYPERTENSIVE HEART DISEASE AND HYPERTROPHIC CARDIOMYOPATHY USING PERSONALIZED 3D MODELING AND CARDIAC MAGNETIC RESONANCE IMAGING

ABSTRACT

Differential diagnosis of hypertensive heart disease (HHD) and hypertrophic cardiomyopathy (HCM) is clinically challenging but important for treatment management. This study aims to phenotype HHD and HCM in 3D+time domain by using a multiparametric motion-corrected personalized modeling algorithm and cardiac magnetic resonance (CMR). 44 CMR data, including 12 healthy, 16 HHD and 16 HCM cases, were examined. Multiple CMR phenotype data consisting of geometric and dynamic variables were extracted globally and regionally from the models over a full cardiac cycle for comparison against the healthy models and clinical reports. Statistical classifications were used to identify the distinctive characteristics and disease subtypes with overlapping functional data, providing insights into the challenges for differential diagnosis of both types of disease. While HCM is characterized by localized extreme hypertrophy of the left ventricular (LV), wall thickening/contraction/strain was found to be normal and in synchrony, though it was occasionally exaggerated at normotrophic/less severely hypertrophic regions during systole to preserve the overall ejection fraction (EF) and systolic functionality. Additionally, we observed that hypertrophy in HHD could also be localized, although in less extreme conditions (i.e. more concentric). While fibrosis occurred mostly in those HCM cases with aortic obstruction, only minority of HHD patients were found to be affected by fibrosis. We demonstrated that subgroups of HHD (i.e. preserved and reduced EF: HHDpEF & HHDrEF) have different 3D+time CMR characteristics. While HHDpEF has cardiac functions in normal range, dilation and heart

failure are indicated in HHDrEF as reflected by low LV wall thickening/contraction/strain and synchrony, as well as much reduced EF.

Keywords: cine MRI; cardiac modeling; hypertensive heart disease (HHD); hypertrophic cardiomyopathy (HCM)

FENOTYPING PENYAKIT JANTUNG HIPERTENSIF DAN KARDIOMYOPATI HIPERTROPIK MENGGUNAKAN PEMODELAN 3D PERSONALISASI DAN GAMBARAN RESONAN MAGNETIK JANTUNG

ABSTRAK

Diagnosis perbezaan penyakit jantung hipertensi (HHD) dan kardiomyopati hipertropik (HCM) secara klinikal masih menghadapi cabaran, tetapi penting untuk pengurusan rawatan. Kajian ini bertujuan untuk membuat fenotype HHD dan HCM dalam domain 3D+masa dengan menggunakan algoritma pembetulan gerakan multiprametrik pemodulatan dan resonans magnetik jantung (CMR). Sejumlah 44 subjek yang melibatkan 12 subjek sihat, 16 pesakit HHD dan 16 pesakit HCM telah dimasukkan dalam kajian ini. Semua data CMR yang mempunyai data informasi secara geometri dan dinamik telah diekstrak secara global dan serantau dari model sepanjang kitaran jantung untuk perbandingan dengan model sihat dan laporan klinikal. Klasifikasi statistik juga digunakan untuk mengenal pasti ciri khas dan subkumpulan penyakit dengan data fungsional yang tumpang tindih dan memberi pandangan mengenai cabaran untuk diagnosis perbezaan kedua-dua jenis penyakit tersebut. Walaupun HCM dicirikan oleh hipertrofi LV ekstrem secara berlokasi, penebalan/pengecutan/ketegangan dinding didapati normal dan selaras, ketebalan kawasan hipertrofik normotrofik/hipertrofi yang serderhana semasa sistol telah ditemui untuk mengekalkan pecahan pelepasan keseluruhan (EF) dan fungsi sistolik. Selain itu, hipertrofi pada HHD juga diiktirafkan secara dilokalisasi pada keadaan yang kurang ekstrem (iaitu lebih sepusat). Dalam kajian ini, fibrosis berlaku pada kebanyakan kes HCM dengan penyumbatan aorta dan hanya sebahagian pesakit HHD yang mempengaruhi fibrosis. Subkumpulan HHD (iaitu EF yang dipelihara dan dikurangkan: HHDpEF & HHDrEF) mempunyai ciri CMR 3D+masa yang berbeza. HHDpEF mempunyai fungsi jantung dalam jarak normal, manakala, pelebaran dan kegagalan jantung telah ditunjukkan dalam HHDrEF seperti yang

ditunjukkan oleh penebalan pengecutan/ketegangan dan ketegangan dinding LV rendah, serta EF yang banyak berkurang.

Kata-kata kunci: cine MRI; pemodelan jantung; model 3D; penyakit jantung hipertensi (HHD); kardiomiophati hipertrofi (HCM)

ACKNOWLEDGEMENTS

First and foremost, I would like to praise and thank God for providing me with the strength and motivation throughout this research. I am extremely grateful to my parents for their unconditional love, caring, support and sacrifices for educating and preparing me for my future.

Above all, I would like to express my deep and sincere gratitude to my research supervisor, Ir. Dr. Liew Yih Miin for giving me this opportunity to carry out this research and providing invaluable guidance throughout this project. Besides, I would like to thank my research consultant, Dr. Ashikin, my research co-supervisor Dr. Chew Bee Teng and Dr. Tan Li Kuo as well as Dr. Chiam for their precious time and effort in guiding me to solve every problem in order to progress in this study. It was a great privilege and honor to work and study under their guidance.

Special thanks to all lab-mates who continuously provide me with supports and cheer me up throughout this master study. I would also like to thank my close friends for their encouragement and prayers during my candidature. In addition, I will like to show appreciation to Asma who help me in retrieving data for my research work. The completion of my master study would not have been successful without these awesome people.

TABLE OF CONTENTS

LIST OF FIGURES

LIST OF TABLES

LIST OF SYMBOLS AND ABBREVIATIONS

°	:	Degree
∑	:	Summation
2D	:	Two-dimensional
3D	:	Three-dimensional
AHA	:	American Heart Association
AHA	:	American Heart Association
ANOVA	:	Analysis of Variance
ANOVA	:	Analysis of Variance
AWT	:	Absolute Wall Thickening
AWT	:	Absolute Wall Thickening
BMI	:	Body Mass Index
BMI	:	Body Mass Index
CAD	:	Coronary Artery Disease
CAD	:	Coronary Artery Disease
CFS	:	Correlation Feature Selection
CFS	:	Correlation Feature Selection
CMR	:	Cardiac Magnetic Resonance
CS	:	Circumferential Strain
CS	:	Circumferential Strain
CT	:	Computed Tomography
CT	:	Computed Tomography
DI	:	Dyssynchrony Index
ED	:	End-Diastole

EDV	:	End-Diastolic Volume
EDWT	:	End-Diastolic Wall Thickness
EF	:	Ejection Fraction
ES	:	End-Systole
ESV	:	End-Systolic Volume
ESWT	:	End-Systolic Wall Thickness
FOV	:	Field Of View
FP	:	False Positive
GLA	:	Galactosidase Alpha
HHDpEF	:	Hypertensice Heart Disease with Preserved Ejection Fraction
HHDrEF	:	Hypertensice Heart Disease with Reduced Ejection Fraction
HNOCM	:	Hypertrophic Cardiomyopathy without Aortic Obstruction
HOCM	:	Hypertrophic Cardiomyopathy with Aortic Obstruction
IL-1	:	Interleukin-1
LA	:	Long-Axis
LDDMM	:	Large Deformation Diffeomorphic Metric Mapping
LR	:	Logistic Regression
LS	:	Longitudinal Strain
LVOT	:	Left Ventricular Outflow Tract
M/V	:	Mass-to-Volume Ratio
max EDWT	:	Maximum End-Diastolic Wall Thickness
MCC	:	Matthews Correlation Coefficient
MRI	:	Magnetic Resonance Imaging
NB	:	Naïve Bayes
NN(MLP)	:	Neural Network (Multilayer Perceptron)

p	:	Probability Value
PACs	:	Picture Archiving and Communication System
PRC	:	Precision Recall Curve
RAAS	:	Renin-Angiotensin-Aldosterone System
RF	:	Random Forest
ROC	:	Receiver Operating Characteristics
RS	:	Radial Strain
SA	:	Short-Axis
SAM	:	Systolic Anterior Motion
SI	:	Symmetrical Index
SSFP	:	Steady State Free Precession
SV	:	Stroke Volume
SVM	:	Support Vector Machine
TGF-β1	:	Transforming Growth Factor Beta 1
TI	:	Thickening Index
TNF-α	:	Tumor Necrosis Factor Alpha
TPM1	:	α-Tropomyosin
VT	:	Ventricular Tachyarrhythmia
σ	:	Standard Deviation

LIST OF APPENDICES

CHAPTER 1: INTRODUCTION

Left ventricular hypertrophy (LVH) is an abnormal deformation of cardiac structure in the form of enlargement and thickening of the cardiac wall. Among the diverse pathological causes, hypertensive heart disease (HHD) and hypertrophic cardiomyopathy (HCM) are the two most common etiologies of LVH (Alkema, Spitzer, Soliman, & Loewe, 2016). HHD is caused by the systemic hypertension which later leads to heart failure (Gradman & Alfayoumi, 2006) if left untreated and is frequently encountered in the hypertensive population. In contrast, HCM is a typical genetic cardiomyopathy that gives rise to sudden death with a prevalence of 1:500 in the population (B. J. Maron et al., 1995). The differential diagnosis of these LVH etiologies are difficult as both diseases might presented clinically with similar extents of wall hypertrophy (Sipola et al., 2011). Accurate and early diagnosis of LVH etiology is of paramount important to ensure appropriate treatment management.

To date, diagnosis of HCM is based on wall thickness >15mm in ≥1 myocardial segment from echocardiographic examination, as recommended by international clinical guidelines (Authors/Task Force members et al., 2014). Cases with lesser degrees of wall thickening (13-14mm) require evaluation of other features such as family history and ECG abnormalities to establish diagnosis. CMR has emerged and been recommended by expert groups as standards for cardiac assessment, not limited to LVH. Sipola et al. (2011) found that maximal end-diastolic wall thickness (EDWT) from CMR is a useful measure to differentiate HCM from mild-to-moderate HHD. Rodrigues et al. (2017) found that indexed LV mass (LVM), absence of systolic anterior motion of mitral valve, and absence of mid-wall LGE are significant predictors of HHD for differentiation from HCM, instead of EDWT. Puntmann et al. (2010) found that HHD is characterized by impaired LV global

systolic function due to impaired radial wall thickening of the dilated LV cavity, whereas HCM is characterized by supernormal global systolic function despite heterogeneous reduced wall deformation in association with regional fibrosis. Nevertheless, contradicting results were noted and most of these LVH-related studies relied on visual and manual in-plane 2D analysis of indices from 3D CMR scans (Puntmann et al., 2010; Rodrigues et al., 2017; Sipola et al., 2011) to describe shape and functional differences between HCM and HHD. Visual assessment is prone to variation between clinicians, global indices lack detailed spatial information, while in-plane indices are prone to measurement inconsistency due to acquisition-related variations in imaging plane-to-myocardial wall intersecting angles and motion artifacts (Tobon-Gomez, Butakoff, Yushkevich, Huguet, & Frangi, 2010).

In an effort to reduce ambiguities due to 2D assessment, some researchers have attempted to model the LV from MRI scans in 3D for extracting biomarkers that are useful in cardiac diagnosis. This 3D assessment has proven to be more reproducible and provides detailed functional measurements to elucidate certain spatial defects in LV affected focally by disease (Bicudo et al., 2008; Chuang et al., 2000). Khalid et al. (2019) and Leong et al. (2019) have reported the use of 3D personalized LV models to examine regional thickening, dyssynchrony and fibrosis distribution, but only for cases of myocardial infarction. Tobon-Gomez et al. (2010) studied two techniques to extract wall thickness from 3D LV models and a single feature yielded moderate classification results for three classes consisting of control, HHD and HCM. Ardekani et al. (2016) described an algorithm to assess focal shape variations between HCM and HHD through deformable shape matching with 3D LV mesh models built from CT scans, but no correlation to functional indices was discussed and no classification was performed to discriminate LVH etiologies. To-date, the use of 3D LV modeling techniques to comprehensively

elucidate distinct characteristics of HHD and HCM at various degrees of severity has not been reported. Understanding the distinct characteristics of subgroups of patients which often pose a challenge in differential diagnosis would be helpful to guide future research in discovering useful biomarkers for these patients.

In this research, a 3D+time personalized LV modeling technique was developed and assessed to extract multiple global and regional parameters for improved phenotyping and diagnosis of HHD and HCM. Regional static and dynamic CMR indices were mapped onto the 3D models and American Heart Association (AHA) bullseye diagrams to aid visualization and quantification of both cardiac pathologies. Subgroups of HHD and HCM cases with overlapping anatomical and functional characteristics which reduce the accuracy of differential diagnosis were examined. The cardiac measurements of these patients were compared against healthy subjects and validated against clinical reports. Finally, different classifiers were tested to differentiate between healthy, HHD, and HCM patients as well as their subgroups, and significant biomarkers were elucidated.

1.1 Research Objective

i. To reconstruct precise 3D personalized LV models using a motion corrected cardiac modeling technique to facilitate visual and quantitative assessment of LV abnormality for two different LVH phenotypes, i.e. hypertensive heart disease (HHD) and hypertrophic cardiomyopathy (HCM).

ii. To develop the image processing and modeling framework for comprehensive CMR phenotyping of LVH cohort across the full cardiac cycle and to compare against the healthy cohort.

iii. To identify the subgroups of HHD and HCM with overlapping features, make recommendations of biomarkers useful to distinguish these phenotypes and, to grade the severity of the hypertrophic conditions.

1.2 Hypothesis

It was hypothesized that both HHD and HCM have abnormal spatial pattern of wall thickness and thickening dynamics as well as strain. These abnormalities could be better demonstrated in 3D+time domain as compared to previous 2D and 3D analysis at specific cardiac phases.

1.3 Scope of Work

The research work was divided into three phases. The first phase comprised data acquisition from the picture archiving and communication system (PACS) of University of Malaya Medical Centre, and segmentation of cine MRI images from healthy subjects, HHD and HCM cohorts.

At the second phase, an image processing and modeling technique was developed and adapted for the reconstruction of 3D+time personalized LV models from the subjects across the full cardiac cycle. The LV mesh models were generated after motion correction via a multi-slice 3D rigid image registration algorithm. A fully automated 3D wall thickness and strain assessment algorithm was subsequently developed and used to compute and generate color-coded 3D wall thickness/strain models across the full cardiac cycle. The models were then split and remapped onto the 17 AHA bullseye diagram to facilitate spatial quantification and visualization of segmental motion and synchrony for each patient. Following this, all LV indices including global functional parameters (i.e. LV mass, EF, EDV, ESV and etc.) and regional parameters (e.g. max EDWT, AWT, TI, DI, SI and myocardial strain) were summarized with respect to 5 groups consisting of the healthy subjects, HHD with preserved and reduced ejection fraction (HHDpEF and

HHDrEF) and HCM with and without aortic obstruction (HOCM and HNOCM). Statistical analysis was performed to identify the significant difference between groups and subgroups and the results were verified using clinical reports.

At the final phase, all global and regional functional data were tested by using various classifiers to identify the subgroups of patients with overlapping cardiac features. Attribute selection technique was utilized to further determine the biomarkers which were significant for the prediction of healthy, HHD and HCM cases.

1.4 Thesis Organization

Chapter 1 conveys a general introduction of this study. This section briefly summarizes the importance and challenges for the diagnosis of LVH etiologies in current clinics. Various existing methods to differentiate HHD and HCM, and gaps of research are briefly discussed and defined. Objective and scope of this research are also presented.

Chapter 2 is the literature review that provides background information on the etiologies of LVH and their clinical assessment. Imaging strategies and computational techniques proposed by other research groups pertaining to phenotyping and analysis of LVH are also presented. These include the imaging and diagnosis modalities, risk stratification of HHD and HCM cases, 3D LV model reconstruction techniques, as well as the global and regional functional assessment.

Chapter 3 explains the methodology proposed by this research to comprehensively phenotype HHD and HCM in 3D and across time domain. This chapter elaborates on the protocol used for 3D motion corrected reconstruction of LV models and automated spatial analysis of functional parameters from the models. This is followed by a detailed description of the statistical analysis and classification of the cases.

Chapter 4 and 5 report and discuss the results of this study as well as compare the findings with previous research. Chapter 6 concludes this research and provides recommendation for future study.

CHAPTER 2: LITERATURE REVIEW

2.1 Left Ventricular Hypertrophy

Left ventricular hypertrophy (LVH) is a cardiac abnormality which manifests as the enlargement and thickening of the myocardial wall. The development of hypertrophy could be due to multitude of factors, with majority of the cases being due to hypertension, family history, aging, neurohormonal stimulation, and environment factors.

One of the crucial factors leading to myocardial hypertrophy is systemic high blood pressure or hypertension. According to the Malaysian Ministry of Health Report in 2008, there is a striking increase in the prevalence of hypertension from 33% to 43% over the past decades. If left untreated, LVH is one of the most potent outcomes of hypertension, leading to a high cardiovascular mortality rate of 30% (Kearney et al., 2005). Moreover, the Framingham study (LEVY et al., 1988) showed that there is a higher risk of LVH in the hypertensive population aged over 70 years old compared to the younger hypertensive population at 30 years old (43% versus 6%). It is believed that LVH is a mechanism to minimize wall stress in response to pressure-overload caused by elevated blood pressure (HHD), as well as in athletic hearts and aortic stenosis.

Apart from the extrinsic factors mentioned above, LVH could also be caused by a diverse range of intrinsic factors. Hypertrophic cardiomyopathy (HCM), for example, is caused by mutations in the contractile sarcomeric proteins that lead to hypertrophy and disarray of myocytes. Anderson-Fabry disease is associated with mutations in the GLA gene. This results in X-linked lysosomal storage disorder and deficiency in the production of enzyme alpha-galactosidase, leading to accumulation of globotriaosylceramide in the myocardium and therefore LVH. Amyloidosis and sarcoidosis, on the other hand, are caused by the deposition of abnormal proteins within the myocardium due to focal

inflammatory process that stimulated aggressive cellular immune response to antigens or self-antigens.

2.2 Hypertensive Heart Disease versus Hypertrophic Cardiomyopathy

Among all the etiologies, HHD and HCM are the two most common phenotypes of LVH affecting Malaysian population. However, differential diagnosis of these diseases is a common clinical conundrum.

HCM is a genetic-related cardiovascular disease which often causes sudden death. It is clinically diagnosed on the basis of localized hypertrophy of the LV with non-dilated and hyper-dynamic myocardium. The inherited pattern of HCM is known to be autosomal dominant due to mutation in one of the sarcomere genes, leading to potential heirs in a family with strong history of HCM. Mutation occurs on the gene which encodes the protein component of sarcomeres that forms both thin and thick filaments (Amin, Chiam, & Varathan, 2019). According to a prior study, the genetic mutation was known to occur on D175 of the α-tropomyosin gene (TPM1) which is associated with the characteristics of extreme LV maximal wall thickness (Sipola et al., 2011). The hypertrophic regions could be accompanied by diffused myocardial fibrosis that decelerate biological cardiac function and performance, causing an increase of ventricular stiffness that leads to abnormal diastolic relaxation (Popović et al., 2008; Urbano-Moral, Rowin, Maron, Crean, & Pandian, 2013; Xu et al., 2017). Nevertheless, over 500 types of mutation in 10 sarcomeric genes have been discovered to date for HCM and no particular clinical HCM phenotype is mutation-specific (Sipola et al., 2011), therefore exhibiting anatomical changes which are highly variable (including variable extent of wall hypertrophy and the presence/absence of aortic obstruction). Additionally, HCM could co-exist with systematic hypertension which adds another level of complexity to its diagnosis.

Hypertensive heart disease (HHD), on the other hand, is caused by systemic hypertension and potentially leading to heart failure, cardiac sudden death, ventricular arrhythmias and coronary artery disease. Hypertension affects approximately 25% of the population worldwide (Kearney, Whelton, Reynolds, Whelton, & He, 2004) and HHD is normally formed after prolonged and severe hypertension. HHD is clinically presented with thickened and enlarged heart, and the extent of wall hypertrophy could vary with the severity of hypertension. Severe HHD with extreme hypertrophy of wall thickness ≥20mm is therefore possible, which exceeds the reference cut-off point of ≥15mm for the identification of HCM (Sipola et al., 2010). Apart from systemic hypertension, hormones and cytokines such as the renin-angiotensin-aldosterone system (RAAS), transforming growth factor beta 1 (TGF-β1), tumor necrosis factor alpha (TNF-α), and interleukin-1 (IL-1) are the non-hemodynamic determinants that influence HHD by promoting fibrosis and inflammatory environment around the heart chamber (Berk, Fujiwara, & Lehoux, 2007; Sun et al., 2019). These results change cardiac cellularity (perivascular inflammation), causing myocardial stiffness, and abnormal contractility and relaxation mechanisms. HHD is also known to cause diastolic dysfunction of the LV despite normal systolic function (i.e. normal ejection fraction). The reason of such abnormality is unclear, potentially linked to defects in motion mechanism which remains to be investigated. Additionally, the grey area of overlap between HCM and HHD as well as their subgroups remains to be studied and the important biomarkers for their differentiation remains to be identified.

2.3 Importance of Accurate Differential Diagnosis

Accurate and early diagnosis of LVH etiology is of paramount importance to ensure appropriate patient management. In general, HHD patients are treated with pharmacotherapy. This includes antihypertensive treatment along with lifestyle change in

terms of dietary modification (e.g. reduce sodium intake), regular aerobic exercise and weight loss. These are crucial to maintain a normal blood pressure (BP) and prevent the occurrence of HHD. With a 5 mmHg reduction in systolic BP, the mortality rate due to stroke could be reduced by 14% and the incidence of coronary artery disease (CAD) and all-cause cardiac diseases could be reduced by 9% and 7%, respectively (Whelton et al., 2002).

Meanwhile, HCM is usually managed with pharmacological and invasive treatments. Beta-blockers (β-blockers) are the most popular and effective agents utilized for pharmacological treatment of HCM cases (Ammirati et al., 2016). The combination of β-blockers and disopyramide (a negative inotropic agent) are mostly used to minimize the symptoms in HCM patients with left ventricular outflow tract (LVOT) obstruction (Marian & Braunwald, 2017). As for invasive treatment, myectomy is normally performed. Other treatments also include implanting a defibrillator to reduce the risk of sudden death, alcohol septal ablation that provides permanent reversal of heart failure in HCM patients with outflow obstruction, heart transplants for non-obstructive end-stage cases, as well as anticoagulant therapy to prevent embolic stroke caused by atrial fibrillation (B. J. Maron, 2018). Gene replacement therapy was also suggested to manage certain HCM cases associated with low levels of mutation or absence of the corresponding protein (Prondzynski, Mearini, & Carrier, 2019).

The different treatment regimens for HHD and HCM clearly indicate that accurate and reliable diagnosis is important to avoid unnecessary aggressive procedures (e.g. surgery) when pharmacotherapy alone is sufficient.

2.4 Clinical Assessment and Limitations

Echocardiography is the most commonly used modality for cardiac assessment. Echocardiography offers some advantages compared to other modalities with respect to the accessibility, lack of radiation exposure and high temporal resolution (Alkema et al., 2016; Squeri et al., 2017). Diagnosis of LVH involves manual measurements of LV wall thickness and quantification of cardiac function in HHD and HCM population with real-time 2D or 3D echocardiography (Bicudo et al., 2008). Several parameters including LV mass and LV geometry are important for the assessment of LVH severity. 2D echocardiography was vital in evaluating EF despite its relative inaccuracy and low reproducibility. However, comparing 2D echocardiography with volumetric echocardiography and MRI, better results for the latter modalities were demonstrated when stratifying healthy subjects and evaluating patient's systolic function (Chuang et al., 2000). Echocardiography examinations, however, are often jeopardized by technical inadequacy (B. J. Maron, 2002), i.e. it is highly operator dependent (Tavakoli & Amini, 2013) and therefore results in weaker correlation in its wall thickness and LV mass measurements as compared to CMR and CT (Alkema et al., 2016). Other limitations include unclear endocardial borders due to speckle noise, limited acoustic window due to the position of the heart behind the rib cage and unreliable geometrical assumptions for volumetric measurements from 2D echocardiography (Squeri et al., 2017).

Cardiac CT has also been used as an option to facilitate the diagnosis of LVH in patients with contraindications for MRI (e.g. patients with cardiac pacemaker) (Zhao, Ma, Feuchtner, Zhang, & Fan, 2014). CT relies on the use of x-rays to image the heart and to produce 3D images of diagnostic quality, with better spatial resolution than MRI (Spartera, Damascelli, Mozes, De Cobelli, & La Canna, 2017). Assessment of global and regional functions as well as LV geometry is feasible. Most cardiac CT scanners are also

equipped with myocardial delay enhancement (MDE) techniques to access myocardial fibrosis. In spite of this, cardiac CT is the least preferred technique for LVH assessment due to several constraints arising from ionizing radiation exposure, contraindications for contrast medium, and relatively low temporal resolution (CNR) (Alkema et al., 2016). Several studies demonstrate significant overestimation of LV volumes (Squeri et al., 2017) as well as slightly overestimated LV wall thickness due to extreme hypertrophy (Zhao, Ma, Feuchtner, Zhang, & Fan, 2014).

Among all modalities, MRI is considered the de facto standard for the assessment of various aspects of cardiac diseases as recommended by expert groups (Authors/Task Force members et al., 2014). Compared to other imaging modalities, MRI provides significantly better image quality in terms of signal-to-noise ratio, less operator-dependency, and it is not constrained by the availability of acoustic window as in echocardiography (Chun et al., 2010). Several MR imaging techniques are useful for cardiac assessment. Specifically, the steady state free precession (SSFP) technique is commonly used for cine imaging and functional measurements as it provides high contrast between myocardium and blood pool (Pennell et al., 2004). In cases of unexplained left ventricular hypertrophy not diagnostic of HCM, current guidelines recommend that strain imaging could make a diagnosis (Authors/Task Force members et al., 2014). Late gadolinium enhancement (LGE) MR scan, on the other hand, is used to assess myocardial scarring or fibrosis. Myocardial scarring or fibrosis has been found to be one of the risk factors in distinguishing between HHD and HCM (Rodrigues et al., 2017). According to Bruder et al. (2010), nearly 70% of the HCM population presented with myocardial fibrosis have their fibrosis confined within the hypertrophic region at the mid-ventricle. Previous studies have also shown that regional impairment of contractility is

predominantly related to the extent of hypertrophy (Urbano-Moral et al., 2013), due to cellular changes in structure and function (Swoboda et al., 2017).

Clinical assessment, nevertheless, is restricted to measurements of global LV functions (e.g. blood volumes, ejection fraction, LV mass) and wall thickness. The adoption of single ventricular geometry index, i.e. wall thickness>15mm at end-diastolic phase to distinguish HCM from HHD (Ardekani et al., 2016; Noureldin et al., 2012; Popović et al., 2008; Urbano-Moral et al., 2013) is poor and subject to failure for severe cases. In addition, most measurement were predominantly performed in 2D, only on 3 sparse short-axis cine slices, and/or restricted to few manual localized measurements. Slice displacement is known to contribute to errors in functional measurements especially when displacement occurs due to inconsistent breath-hold position and patient's motion (Y. Liew et al., 2015). Overestimation of wall thickness is also a common issue in 2D due to its dependency on perpendicular image-to-wall intersection (Beohar et al., 2007; Sheehan et al., 1986; van der Geest, de Roos, van der Wall, & Reiber, 1997). Such 2D analysis also ignored longitudinal shortening, which could potentially result in imprecise assessment of functions across phases (Bhan et al., 2014). Therefore, current clinical measures have been found to be not always sufficiently reliable, sensitive or specific. Although cine covers 20-30 phases of the cardiac cycle, only the end-diastolic and end-systolic frames are routinely manually assessed using a highly time-consuming post-processing framework. Only about 7-10% of ≈ 300 cross-sectional scans per patient are used in practice to extract quantitative measures for diagnosis, while the rest are unused or assessed just visually. Research is therefore required and ongoing to utilize the entire data set (covering the entire LV and across all phases), construct 3D models for detailed regional functional assessment, identify "grey areas of overlap" as well as to extract and identify the most persuasive, dominant and significant set of biomarkers to phenotype and

discriminate HHD from HCM. Accurate assessment aids clinical decision in selecting appropriate treatments and to prevent surgical procedures with higher risk of danger.

2.5 Model Reconstructions for Cardiac Assessment and Diagnosis

Back in 2000, Chuang et al. (2000) published a study on 3D reconstruction technique in determining the ventricular strain of gene-targeted mice using tagged MRI. They found that the reconstructed 3D model (Figure 2.1) mimicked the entire myocardial structure and could contribute to more accurate measurement of LV functions. The cardiac myofiber geometry model was built and the wall thickness and strain measurements were extracted. Their technique was capable to identify abnormal myocardial strain pattern in the LV. Regional mechanical dysfunction in the form of the attenuation on both end-systolic radial strain and torsional shear was observed in the engineered mouse. Nevertheless, the focus was on strain analysis on the genetically engineered mice with dilated cardiomyopathy.

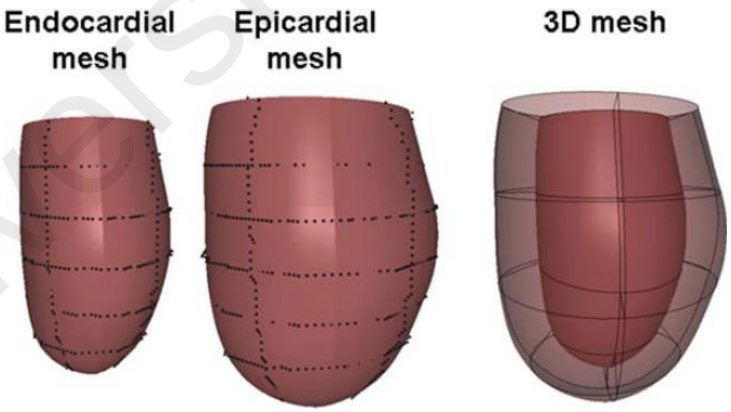

Figure 2.1: The reconstruction of LV 3D mouse model by fusing both endocardial and epicardial meshes (Chuang et al., 2000).

In year 2002, an automatic extraction of corresponding landmarks in 3D shapes and reconstruction of 3D statistical models for quantitative assessment of left and right ventricular heart chambers were demonstrated by Frangi, Rueckert, Schnabel, and

Niessen (2002). Moreover, a multiresolution free-form non-rigid registration algorithm (continuous deformation of B-spline functions) were utilized to find correspondences between shapes. Fourteen healthy subjects were used in the construction of atlas models. The approach provided promising results with an average accuracy and precision of 2.2mm and 1.5mm, respectively, for landmark placement. Nevertheless, this matching technique might cause error while building models of normal and abnormal structures due to different disease states yet to be investigated.

In 2010, Tobon-Gomez et al. (2010) demostrated the 3D model reconstruction technique to discriminate between HHD and HCM by using LV wall thickness at end-diastolic phase. Normal and medial techniques were compared for wall thickness extraction (Figure 2.2 (a) & (b)). It was found that the normal approach had higher accuracy in HCM, while the medial approach achieved better classification accuracy in HHD. The normal surface measurement technique tended to overestimate wall thickness especially in high curvature regions of the heart. The limitation of this study is that only a single cardiac phase was analyzed, i.e. end-diastolic phase. There was no assessment on how various hypertrophic conditions affect the dynamics or movement of the LV wall, which may provide added value for differentiating HHD from HCM.

(a) (b)

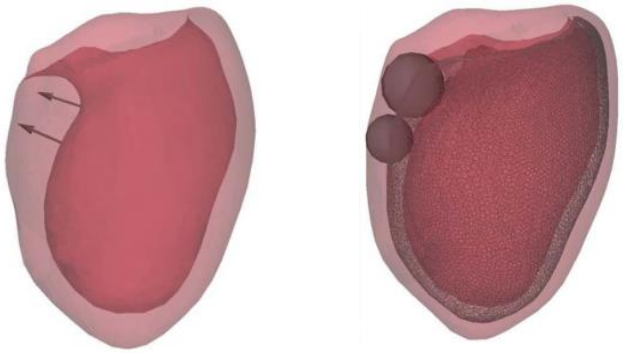

Figure 2.2: (a) Normal measurement technique for wall thickness extraction from both endo- and epicardial surface. (b) Medial measurement technique measures the wall thickness as the length of the radii of maximally inscribed sphere (Tobon-Gomez et al., 2010).

de Marvao et al. (2014) developed a multi-atlas technique that utilize prior data from a set of manually segmented cardiac MR images to evaluate the feasibility and accuracy of high spatial resolution 3D cine imaging for phenotypic analysis of the LV in the healthy population. Multi-atlas PatchMatch algorithm was utilized to match corresponding patches from 20 atlases to the target images, which had been marked manually to facilitate automatic segmentation. Co-registration was later applied to all segmented images to reconstruct a 3D model with consistent spatial coordinates. Although the 3D models provided encouraging quantification, only short-axis cine images were used in their analysis and only ED-to-ES shape variation (i.e. 2 cardiac phases) was explored. Overall, this study developed an automatic segmentation technique for the reconstruction of 3D LV model but this technique has yet to be implemented on patients who were diagnosed with HHD and HCM. Nevertheless, these studies encourage the exploration of both long and short-axis cine images at various time frames to bring insight into spatial wall thickness and dynamics of the LV under various hypertrophic conditions.

Corden et al. (2016) and Ardekani et al. (2016) have proposed similar techniques in the reconstruction of 3D LV models by interpolating the labelled atlas to extract global

cardiac features. However, Corden et al. (2016) study only focused on the relationship between body composition and LV geometry without involving CAD patients. Ardekani et al. (2016), in contrast, has developed 3D LV model by consolidating cardiac CT images with MRI images in order to differentiate HHD from HCM. They used the large deformation diffeomorphic metric mapping (LDDMM) method to register the shape of interest to the LV surface template by surface-to-curve matching. The LV template was reconstructed from the multi-detector CT images. The regional shape variations were examined on both static and dynamic ES and ED cardiac phase to distinguish between HHD and HCM. Their results reveal more pronounced regional shape difference at ES phase than ED phase between HHD and HCM. Larger radial geometrical strain was determined in HCM patients as compared to HHD patients. This study only made use of short-axis cine images for surface-to-curve matching, and was likely prone to inaccuracy caused by patient motion as no correction or slice misalignment was incorporated into the framework.

2.6 Biomarkers of HHD and HCM

Differentiating between HHD and HCM is a complex and challenging task for the clinicians as both of these LVH phenotypes have heterogeneous characteristics that occasionally overlap each other. Global functional assessment alone is insufficient as LV could demonstrate normal global functional values such as ejection fraction, blood volume and LV mass despite of the presence of local abnormality. Regional assessment of the cardiac functions and contractility may shine some lights on this to reduce incidences of misdiagnosis and improper treatment that likely lead to lethal events. Therefore, several studies have focused on identifying the key functional characteristics that are distinctive between these two patient populations.

Nearly three decades ago, Keller et al. (1990) carried out a study to compare the LV morphological structure from M-mode (one-dimensional) echocardiography and 2-D echocardiography to distinguish HHD and HCM. Measurements that were suggested as predictors for these phenotypes included LV segmental wall thickness, LV dimension during ES and ED, ratio of the interventricular septum wall thickness to the posterior wall thickness, the area of myocardial ring and LV mass index. They have found that 80% of the septal and anterolateral free wall regions of the LV were hypertrophied in HHD patients. The degree of asymmetric hypertrophy was suggested as a good indicator to distinguish HCM from HHD.

Twenty-years later in 2011, Sipola et al. (2011) studied various measurements to discriminate HHD and HCM by using cardiac MR imaging. Comparison was made between patients with HCM and patients with mild-to-moderate hypertension. The LV wall was stratified into several segments and measurements were taken including the maximal wall thickness, septum thickness and septum-to-lateral wall thickness ratio. HCM patients were found to have significantly greater LV wall thickness throughout the evaluated segments than HHD. In contrast, LV mass and end-diastolic volume index failed in discriminating these patient groups. The non-discriminatory property of LV mass was further shown by Sanaani and Fuisz (2019) where a majority of the HCM population demonstrated normal LV mass. The study was limited to mild-to-moderate HHD which normally exhibits lesser wall thickness than HCM patients. Some severe HHD cases could have extreme hypertrophy (≥ 20mm) that overlap or even exceed the study's proposed cut-off point of ≥17mm for the identification of HCM.

Puntmann et al. (2010) and Sun et al. (2019) on the other hand, evaluated myocardial strain and the presence of fibrosis as indicators to distinguish HHD and HCM. These studies demonstrated significant reduction of longitudinal strains (over other strain such as circumferential and radial strain) in HCM patients especially in hypertrophic segments. The amount of myocardial fibrosis was found closely related to the extent of hypertrophy, and the fibrosis was found contributing to the attenuation of myocardial shortening in HCM. Bruder et al. (2010) showed complementary results with nearly 70% of their HCM patients having hyper-enhancement in LGE scans (Figure 2.3). Spartera et al. (2017) corroborated the relationship between the extent of myocardial fibrosis and abnormality in myocardial deformation in the form of myocardial strain. Additionally, Puntmann et al. (2010) concluded that HHD patients were characterized by impaired LV global systolic function due to impaired radial wall thickening of the dilated LV cavity as well as increased LV stress.

(a) (b)

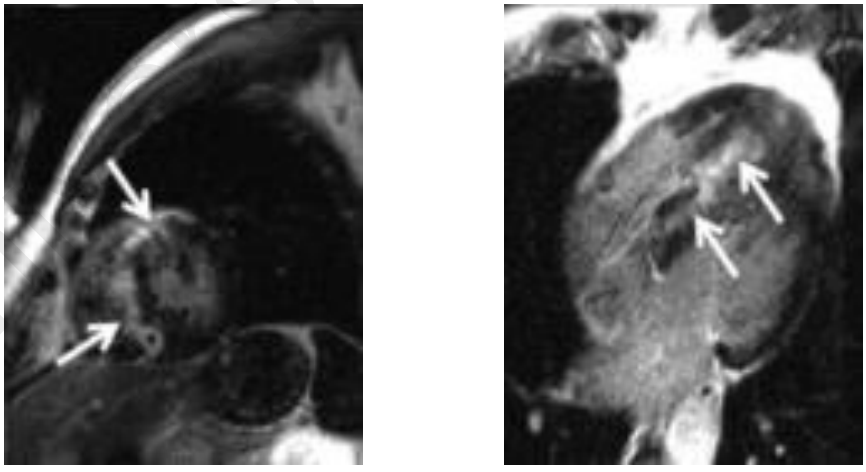

Figure 2.3: LGE scans for the detection of extensive scaring (white arrows) on both (a) short-axis and (b) long-axis left ventricular cine MR images in HCM patient (Bruder et al., 2010).

In 2016, Rodrigues et al. (2016) demonstrated various alternative measurements on LV wall thickness and strain. The impact of end-diastolic wall thickness (EDWT), end-systolic wall thickness (ESWT), myocardial strain, mid-wall circumferential fractional shortening and LV ejection fraction were evaluated on HHD patients. They concluded that EF is a weak indicator of LVH, while the wall thickness and myocardial contractility are important factors for the diagnosis. Increase of EDWT was linearly correlated with the attenuation of longitudinal and circumferential shortening. The absolute wall thickening (AWT) from ES to ED phases was found a better surrogate for thickness analysis. This study concluded that HHD does not have significant LV systolic dysfunction as EF remains in a normal range.

In the subsequent year, multiple variables were explored by the same research group to compare HHD against HCM (Rodrigues et al., 2017). HCM patients were identified by their greater LV wall thickness of more than 15mm at any level of myocardial segment. The extreme hypertrophy was also highly likely to yield asymmetrical walls (Tsang, Chan, Shiu, Lee, & Chan, 2018). Other parameters included in this study were the body mass index (BMI), LV mass, LV symmetry, systolic anterior motion of the mitral valve (SAM) and myocardial fibrosis. HHD patient were prone to have a greater BMI, higher LVM index and no mid-wall enhancement in LGE. On the other hand, 38% of LGE visualizing myocardial fibrosis were identified in HCM patient and only 4% in HHD. Meanwhile, there was a significant difference in the presence of SAM between the HCM (41%) and HHD (0%) populations. Although HCM showed greater maximal asymmetrical wall thickness, LV geometry was deemed a weak predictor for both cases as a minority of HHD patients also presented with asymmetrical LV characteristics (Figure 2.4). This research concluded that mid-wall fibrosis is an outstanding discriminator between HHD and HCM in myocardial segments with wall thickness

≥15mm during ED phase (Figure 2.5). It was recommended that biopsy or genetic procedure should be performed concurrently to supplement the clinical diagnosis.

(a) (b)

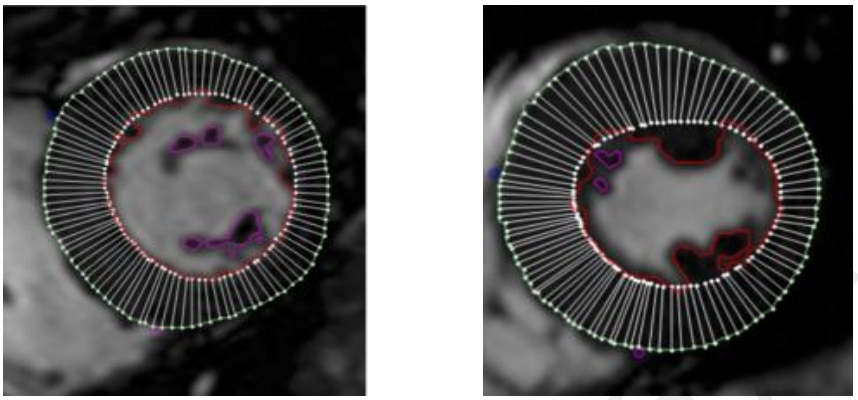

Figure 2.4: Steady state free precession (SSFP) mid short-axis cine images at end-diastole show asymmetrical LV in both HHD patients (a) and HCM patient (b) (Rodrigues et al., 2017).

(a) (b)

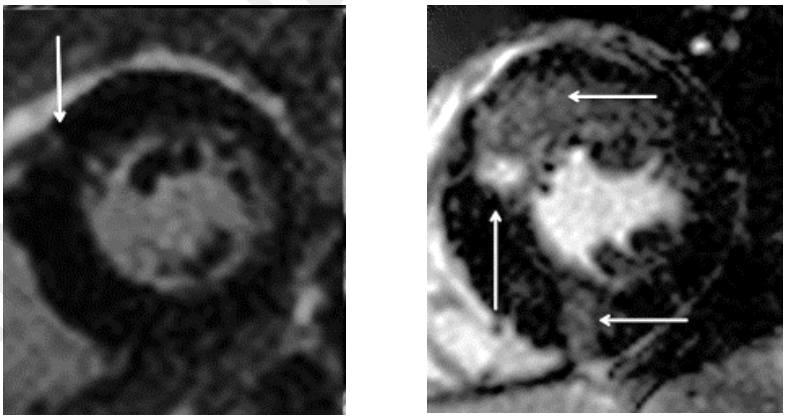

Figure 2.5: (a) Focal fibrosis in HHD patient (b) dispersed fibrosis in HCM patient throughout the myocardium. Fibrosis in the LGE scans are indicated by the arrows (Rodrigues et al., 2017).

In recent years, machine learning techniques, specifically data mining techniques, have been employed to identify significant features for the prediction of heart diseases. Analyses were performed on huge number of raw data sets and provide promising statistical information for clinical decision and predication. Amin et al. (2019)

demonstrated the used of 7 classification techniques including k-NN, Decision Tree, Naïve Bayes, Logistic Regression, Vote, Support Vector Machine and Neural Network to determine the crucial attributes in diagnosing heart diseases from the UCI Cleveland dataset. The results were then later evaluated using UCI Statlog dataset and an accuracy of 87.4% was achieved. This study only input the demographic data for prediction and did not incorporate geometrical data from MRI nor LVH etiologies as the prediction outcome. In 2020, Alis, Guler, Yergin, and Asmakutlu (2020) used machine learning-based texture analysis on LGE scans for the assessment of ventricular tachyarrhythmia (VT) in HCM patients. A promising accuracy of 94.1% was achieved to correctly classify the VT-positive patients VT-negative patients. Nevertheless, the application of machine learning techniques on LVH remains to be investigated to provide further information on significant features for the accurate diagnosis and prediction of its phenotypes.

2.7 Summary

The literature has been reviewed indicating a significant gap in the assessment of cardiac functions for phenotyping and differential diagnosis of HHD and HCM. Cardiac MRI is considered a gold standard in the assessment of cardiac functions. However, current clinical assessment from cardiac MRI scans still pretty much restricted to 2D manual assessment, which is rather subjective and time consuming. Clinical assessment using EF and maximal EDWT has been shown to be non-specific and insufficiently sensitive to distinguish both phenotypes of LVH under study. None of the previous studies has identified the subgroups of patients affected by HHD and HCM which have similar or overlapping LV characteristics that impede accurate differential diagnosis. Recent developments (Ardekani et al., 2016; Tobon-Gomez et al., 2010), nevertheless, have demonstrated that useful insights are possible with more advanced 3D modeling and classification techniques to phenotype and aid in the diagnosis of different diseases.

In this study, it was hypothesized that both HHD and HCM could demonstrate abnormal spatial pattern of wall thickness and thickening dynamics as well as strain which are better depicted in 3D+time domain (as compared to previous 2D and 3D analysis at specific cardiac phases). A personalized 3D cardiac modeling framework was therefore developed and evaluated to phenotype the geometrical and contractility abnormality in patients, specifically for the 2 main LVH phenotypes, i.e. HHD and HCM. A comprehensive set of multiparametric measurements were extracted out from 3D models generated across the full cardiac cycle (i.e. 20 phases) as opposed to only 2 cardiac phases (i.e. ED and ES phases). The measurements included both global and regional functional indices to better quantify the phenotypical difference between HHD and HCM. These indices were displayed both in 3D+time models and bullseye diagram to facilitate visual and quantitative assessment across phases. The measurements were validated with clinical MRI reports and compared using statistical analysis. Classification techniques were explored to classify the disease and to select significant biomarkers. Subgroups of patient that pose a challenge in the differential diagnosis were revealed. This is the first attempt of using 3D+time LV remodeling algorithm and cine MRI across full cardiac cycle to explore and provide insights of the phenotypical difference between HHD and HCM, with the ultimate goal to aid accurate and fast clinical diagnosis for better patient management. The proposed method is described in detail in the next chapter.

CHAPTER 3: METHODOLOGY

3.1 Study Population and Data Acquisition

Cardiac MRI scans of 16 HHD and 16 HCM patients were retrieved from PACS in the University of Malaya Medical Centre. This consisted of standard short-axis (SA) cine stacks covering from base to apex, as well as 2-chamber and 4-chamber long-axis cine (LA) scans. These patients were diagnosed clinically based on echocardiographic/ECG/CMR diagnostic criteria for HCM & HHD. All HCM patients had an expressed LV phenotype, and was diagnosed based on demonstration of a non-dilated, hyperdynamic hypertrophied LV of ≥15 mm in thickness ≥1 myocardial segment without presence of another cardiac or systemic disease that could result in hypertrophy of similar magnitude. Neither endomyocardial biopsy nor genetic testing was used to reach diagnosis. HHD patients were diagnosed based on evidence of treated essential hypertension (blood pressure at systole of ≥140mmHg and at diastole of ≥95mmHg) and increased LV mass index on CMR (>89g/m^2 in men and >73g/m^2 in women) without secondary causes for elevated blood pressure leading to LV hypertrophy, such as family history of HCM or sudden death (Alfakih et al., 2003).

All MRI scans were acquired using a 1.5T MRI system (Signa HDxt 1.5T, GE Healthcare, WI, U.S.A). Specifically, SA cine scans were multi-breath-hold SSFP scans with FOV of 350×350mm, 256×256 image matrix, pixel size of 1.37×1.37mm, slice thickness of 8mm, 0mm slice gap, TE/TR of 1.6/3.7ms, flip angle of 55°, number of slices 10–15, 20 cardiac time frames, and end-expiration breath-hold time of 15s. The LA cine scans were also prescribed with the same acquisition parameters but depicting both standard 2- and 4-chamber perspectives. The corresponding LGE scans of the patients were also retrieved. These were standard 2D SA inverse recovery fast gradient recalled echo LGE scans, which were collocated with the SA cine scans. The parameters for the

LGE imaging were as follows: TE/TR of 3.0/6.0ms, inversion time of 200–300ms (based on null point of normal myocardium), flip angle of 20˚, FOV=350×350mm^2, image matrix=256×256, pixel size=1.37×1.37mm^2, slice thickness of 8mm, 0mm slice gap, and end-expiration breath-hold time of 18s. Based on the institutional clinical scanning protocol, the delay time was chosen to yield mid- to late-systolic phase images in order to best visualize the presence of fibrosis especially sub-endocardial fibrosis when the myocardium is at its full extended thickness (Pennell, 2002). For control, 12 age-matched healthy subjects with normal cardiac functions and no cardiovascular disease as determined by echocardiography were recruited separately with prior informed consent. The standard clinical cine scanning protocol was used and the study was approved by the Institutional Ethics Committee (989.75).

3.2 3D Modeling, Functional Assessment and Disease Classification

In this research, a 3D+time LV modeling algorithm is proposed to study global and regional functions of the LV in HHD and HCM patients for their discrimination, and to compare the measurements against healthy subjects. The algorithm is illustrated in Figure 3.1 and consists of three main stages: 1) Segmentation and reconstruction of 3D+time personalized LV models; 2) Extract of global and regional phenotype data from 3D models; 3) Statistical analysis and classification for inference of phenotype relationships.

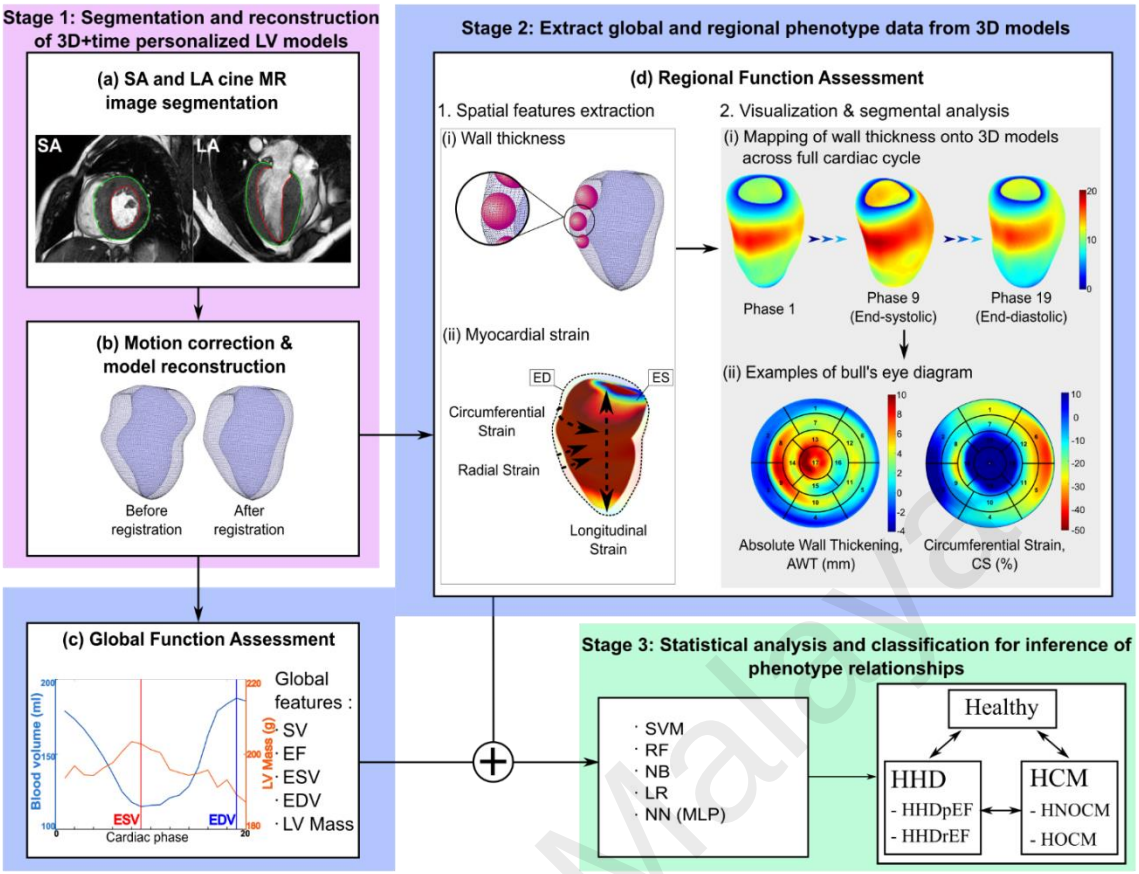

Figure 3.1: The 3D+time personalized LV modeling framework for the phenotyping of LVH from CMR scans. The first stage is the segmentation and reconstruction of 3D LV models, followed by the extraction of global and regional data and finally the statistical analysis and classification.

3.2.1 Stage 1: Segmentation and Reconstruction of 3D+time Personalized LV Models

To reconstruct the LV model, epi- and endocardial contours were semi-automatically delineated. Specifically the SA images were processed through an in-house fully automated LV segmentation algorithm based on convolutional network regression (Tan, Liew, Lim, & McLaughlin, 2017; Tan, McLaughlin, Lim, Abdul Aziz, & Liew, 2018). This was followed by manual corrections of the SA contours where necessary by using the research version of Segment software (Medviso AB; Version: 2.1 R6078) (Heiberg et al., 2010), as well as manual delineation of LV from LA images using the same software (Figure 3.1(a)). An automated boundary detection tool was utilized to aid the

segmentation process with corrections where necessary. Papillary muscles and blood pool were excluded from myocardium for the delineation. An in-house multi-slice rigid image registration algorithm was subsequently applied to correct for 3D translational and rotational misalignment between SA and LA slices due to motion artifacts. Motion corrected SA and LA contours were built into a series of 3D LV surface models for each individual patient by fitting the contours with closed and open cubic B-spline curves across all cardiac phases. The resulting models consisted of epi- and endocardial walls, each in the form of a quadrilateral surface mesh with 101×101 vertices (Figure 3.1(b)). The registration and model building algorithms are detailed in (Khalid et al., 2019).

3.2.2 Stage 2: Extraction of Global and Phenotype Data from 3D Models

(a) ***Global functions***

Global indices were automatically extracted from the 3D LV models. These include end-diastolic volume (EDV), end-systolic volume (ESV), stroke-volume (SV), ejection fraction (EF) and LV mass. EDV and ESV, in ml, were computed from the endocardial surface using surface integration based on the divergence theorem (Kreyszig, 2009). SV is computed by subtracting ESV from EDV. EF is the amount of blood, in percentage, ejected by the LV during each heartbeat and was computed with Eq. (3.1):

$$EF\ (\%) = \frac{EDV - ESV}{EDV} \times 100\% \tag{3.1}$$

LV mass was computed as the product of the myocardial tissue volume and the specific density of myocardium ($1.05 gcm^{-3}$) (Semelka et al., 1990). Both EDV and mass were subsequently used to calculate mass-to-volume ratio (M/V).

(b) ***Regional functions***

For each individual patient, 20 LV surface mesh models were generated, one per cardiac phase across the full cardiac cycle of 20 phases. Several static and dynamic regional indices were automatically measured from these models, including wall thickness, absolute wall thickening (AWT), time-to-peak and myocardial strains (i.e. radial, circumferential, and longitudinal strains).

Wall thickness was measured spatially on each model. This involved initially computing the medial surface between the epi- and endocardial meshes. At each vertex on the medial surface, 10 neighboring vertices were identified in both the epi- and endocardial meshes (i.e. 5 from each mesh) by adopting k-nearest neighbor method and Euclidean distance measure (Friedman, Bentley, & Finkel, 1977). A sphere was subsequently fitted to these vertices through Nelder-Mead Simplex optimization (Lagarias, Reeds, Wright, & Wright, 1998). The diameter of the fitted sphere was used as the wall thickness measurement. This fitting process (Figure 3.1(d)(1)(i)) was repeated across all vertices on all models across the full cardiac cycle. These spatial measurements were subsequently displayed on the LV surface models (Figure 3.1(d)(2)(i)) with a color scale to facilitate visual and quantitative assessment.

AWT is a measure of wall contractility, providing the amount of wall thickening from ED to ES. It is calculated by subtracting wall thickness at ED phase from ES phase, of which the phases were identified automatically as the time point of minimum and maximum blood volumes, respectively. However, since all the vertices on the surface models from different cardiac phases are not spatially aligned, direct subtraction is error prone. Therefore, mapping onto a common coordinate system in the form of a bullseye diagram (Cerqueira et al., 2002) was implemented before any arithmetic operations were

performed across phases. In the mapping process, each model was split into 17 AHA segments. To split the model, the model was tilted to align with a reference central axis which was computed as the best fit line of the centroids from the epicardial mesh at the first cardiac phase. The apex (segment 17) was first delineated as part of the LV myocardium located below the endocardial wall. The remaining body of the LV was then divided into 3 equal sections consisting of basal, mid and apical. Next, an interior bisector was computed from a triangle formed by two pre-picked RV-LV junction points at the mid-ventricular plane and the intersection point of the central axis with the mid-ventricular plane. The bisector was rotated about the central axis to further divide the LV horizontally resulting in 6:6:4 segments in the basal, mid-ventricular and apical sections, respectively. The wall thickness values were spatially mapped onto the bullseye diagram using linear interpolation. Overall there were 20 bullseye diagrams of wall thickness measurements, one per cardiac phase. The diagrams at the ED and ES phases were subtracted to yield AWT measurements (Figure 3.1(d)(2)(ii)), which could be remapped back onto the 3D model for visual presentation.

Time-to-peak is computed as the time/cardiac phase at which the individual points on the LV wall achieve maximum thickness, in unit % of R-R interval. As with AWT, time-to-peak was extracted directly from the series of bullseye diagrams. The similarity of time-to-peak values across the LV surface is an indication of the degree of synchrony between cardiac segments (especially between septal and lateral free wall), of which high synchrony is required for effective ejection of blood during systole.

Myocardial strain is the % change in myocardial length from relaxed to contractile state, which represents the deformation degree of the myocardial wall (Figure 3.1(d)(1)(ii)) (Pedrizzetti, 2014; Cardim, 2015; Alenezy, 2015; Scatteia, 2017). All

instantaneous strain measurements in this study were computed using the general equation (Eq. 3.2) as follows:

$$Myocardial\ Strain\ (\%) = \frac{L_t - L_o}{L_o} \times 100 \quad (3.2)$$

where L_t is the length after deformation at phase t and L_o is the reference length at ED phase. For radial strain (RS), it was computed as the localized deformation of the myocardial wall in the form of wall thickening/thinning at phase t with reference to the EDWT (i.e. by subtracting the bullseye diagram of wall thickness at phase t from ED phase before dividing by the ED thickness). In contrast, circumferential strain (CS) was derived from the endocardial surface in the form of reduction in its circular perimeter (or radius) towards the center of the LV cavity. This involved generating bullseye diagram of endocardial radius at all phases before computing the difference with respect to the ED phase. Finally, longitudinal strain (LS) was derived as the base-to-apex shortening at the endocardial surface. The endocardial surface was used in the computation of CS and LS because the subendocardial layer has been shown to contribute the most to LV deformation as compared to the mid-myocardium and subepicardial layers (Johnson, Kuyt, Oxborough, & Stout, 2019). Both CS and LS were presented in negative strain values as the myocardial fiber underwent shortening, whereas RS could be positive/negative in values depending on the form of deformation (i.e. thickening/thinning) of the myocardial wall. To aid visual assessment, the LV models were also color-coded spatially with the strain measurements. Such models are a visual means to allow spatial inspection of wall deformation across the cardiac cycle for identifying regional LV contractility defects.

To summarize the overall structural and functional characteristics of the LV for each patient, the following parameters were computed from the mid-to-apical cardiac segments of the bullseye diagrams:

$$TI(mm) = \frac{1}{10}\sum_{i=1}^{10}(T_{ES_i} - T_{ED_i}) \tag{3.3}$$

$$DI(\%) = \frac{\sigma_{time-to-peak}}{20\ phases} \times 100 \tag{3.4}$$

$$\text{RS}\ (\%) = \frac{1}{10}\sum_{i=1}^{10}(RS_{ES_i} - RS_{ED_i}) \tag{3.5}$$

$$\text{CS}\ (\%) = \frac{1}{10}\sum_{i=1}^{10}(CS_{ES_i} - CS_{ED_i}) \tag{3.6}$$

$$\text{LS}(\%) = \frac{L_{ES} - L_{ED}}{L_{ED}} \times 100 \tag{3.7}$$

$$\text{SI} = \frac{T_{max}}{T_{opposite\ min}} \tag{3.8}$$

where *i* represents the cardiac segments (segments 7-16); T_{ES_i} and T_{ED_i} are the average segmental wall thickness at ES and ED phases, respectively; and $\sigma_{time-to-peak}$ is the standard deviation of time to maximum thickness within segments 7-16; RS_{ES_i} and RS_{ED_i} are the average segmental radial strain at ES and ED phases, respectively; CS_{ES_i} and CS_{ED_i} are the average segmental circumferential strain at ES and ED phases, respectively; T_{max} is the maximal wall thickness at ED whereas $T_{opposite\ min}$ is the minimum thickness of the opposite segment at the same phase. TI shows the average amount of maximal changes in thickness value in mm with reference to the ED phase, whereas DI highlights the variation in contraction timings among the segments. SI≥1.5 indicates asymmetrical shape during contraction. The basal segments (segments 1-6) and apex (segment 17) were excluded from these calculations, consistent with clinical assessment, as basal segments

normally show minimal contractility whereas the apex is generally much thinner and prone to model reconstruction error. Finally, regional assessment of fibrosis was performed on LGE scans by using Segment Software, for correlation to the functional values mapped on the bullseye diagram or the 3D LV models. The algorithm was developed in MATLAB (2018a) and implemented on an Intel(R) Core (TM) i5-3570 CPU @3.40 GHz computer. Parallel computing was utilized to accelerate the process. Complete analysis on each subject consumed approximately 8-10 minutes for a full cardiac cycle.

3.2.3 Stage 3: Statistical Analysis and Classification for Inference of Phenotype Relationships

The statistical analysis was implemented using SPSS Version 22. Only 11 out of 15 global and regional CMR phenotype variables were found to be normally distributed tested using a Kolmogorov Smirnov test. Non-parametric Kruskal-Wallis test was performed to identify the significant differences between the groups; the variables were reported in median and interquartile range (IQR) with the significant level set at *p*-value<0.05.

The global and regional CMR phenotype variables computed from a total of 44 participants consisting of 12 healthy, 16 HHD and 16 HCM patients were analyzed through statistical classification to infer relationships between patient groups (i.e. to identify groups/subgroups with overlapping CMR phenotypes). Fifteen CMR phenotype variables were used as input: EDV, ESV, LV mass, max EDWT, SV, EF, TI, DI, mean AWT, SI, presence of fibrosis, RS, CS, LS and M/V. Five statistical models were tested: Random Forest (RF), Support Vector Machine (SVM), Naïve Bayes (NB), Logistic Regression (LR) and Neural Network (Multilayer Perceptron) (NN (MLP)) as indicated

in Figure 3.1(e). Ten-fold cross validation was applied to the datasets for training and testing. The performance of the statistical models was assessed using accuracy, false positive (FP) rate, precision, F-measure, Matthews Correlation Coefficient (MCC), receiver operating characteristics (ROC) area, and precision recall curve (PRC) area. In addition, the 15 CMR phenotype variables were subject to a feature selection process using 5 algorithms: Correlation Feature Selection (CFS), Correlation, Information Gain, Gain Ratio and ReliefF. Among the 15 LV CMR variables, the top 5 most significant parameters to differentiate healthy, HHD and HCM cases were determined.

CHAPTER 4: RESULTS

4.1 Demographic and Functional Comparisons between Healthy, HHD and HCM Patients

The median age (IQR) for 3 groups of patients were 50 (11.8) years-old in healthy, 63 (15.3) years-old in HHD and 56 (22.5) in HCM patients respectively. The male:female gender ratio for healthy subjects was 8:4; HHD was 13:3; and HCM was 11:5. The summary of all the LV functional parameters for the three main groups (healthy, HHD and HCM) and subgroups (HHDpEF, HHDrEF, HOCM and HNOCM) of patients were shown in Table 4.1. Few LV parameters show significant differences between HHD and HCM, including the TI and SI. The LV mass was significantly higher in the HCM and HHD groups as compared to the healthy group. Compared to the healthy group, the HHD group had elevated ESV, whereas the HCM group had elevated M/V ratio.

Table 4.1: Characteristics of the healthy and targeted groups (median (IQR)).

Variables	Healthy (n = 12)	HHD (n = 16)		HCM (n = 16)	
		HHDpEF (n = 6)	HHDrEF (n = 10)	HNOCM (n = 5)	HOCM (n = 11)
ESV (ml)	46.2 (11.3)	28.5 (17.0)	137.1 (75.2)	73.9 (63.4)	41.4 (32.4)
		108.9 (105.1)		53.3 (41.2)	
EDV (ml)	125.3 (10.3)	95.0 (36.5)	214.4 (77.0)	165.0 (51.2)	159.1 (56.2)
		163.2 (102.0)		148.7 (43.9)	
SV (ml)	79.1 (7.5)	66.9 (26.3)	70.5 (21.1)	79.3 (13.3)	81.8 (26.5)
		70.5 (22.3)		80.6 (25.2)	
M/V (g/ml)	0.7 (0.1)	1.1 (0.5)	0.9 (0.3)	1.1 (0.2)	1.5 (0.3)
		0.9 (0.4)		1.3 (0.4)	
Mass (g)	82.8 (15.6)	121.1 (84.4)	176.3 (57.2)	184.7 (14.3)	214.0 (108.3)
		167.6 (50.5)		190.1 (70.3)	
EF (%)	62.4 (4.3)	65.6 (10.9)	32.8 (9.5)	55.2 (21.9)	63.7 (15.6)
		41.4 (34.9)		61.3 (11.8)	
Max EDWT (mm)	9.9 (2.6)	14.9 (5.0)	13.7 (4.4)	15.9 (1.6)	19.0 (4.4)
		14.0 (4.2)		17.6 (4.3)	
TI (mm)	4.7 (0.9)	5.8 (2.0)	2.7 (0.6)	4.8 (1.8)	7.3 (1.9)
		3.0 (2.8)		6.7 (2.7)	
DI (%)	3.0 (0.8)	2.8 (2.1)	4.9 (4.1)	5.5 (2.5)	3.1 (1.9)
		4.5 (3.3)		4.3 (2.6)	
SI	1.2 (0.2)	1.2 (0.2)	1.3 (0.2)	1.6 (0.4)	1.6 (0.6)
		1.2 (0.2)		1.6 (0.6)	
RS (+ %)	88.8 (15.3)	87.5 (33.6)	31.0 (11.0)	52.0 (24.8)	87.7 (30.3)
		39.4 (32.7)		70.0 (42.4)	
CS (- %)	30.3 (13.7)	36.3 (4.6)	14.1 (9.2)	16.9 (13.5)	23.8 (9.6)
		19.7 (20.9)		23.8 (6.8)	
LS (- %)	8.0 (1.2)	4.0 (3.4)	3.5 (1.4)	3.8 (0.004)	5.2 (2.2)
		3.6 (1.5)		4.5 (1.8)	

IQR, interquartile range; ESV, end-systolic volume; EDV, end-diastolic volume; SV, stroke volume; M/V, mass-to-volume ratio; EF, ejection fraction; Max EDWT, maximum end-diastolic wall thickness; TI, thickening index; DI, dyssynchrony index; SI, symmetricity index; RS, radial strain; CS, circumferential strain; LS, longitudinal strain. Statistically significant difference was listed in APPENDIX.

Figure 4.1 depicts the difference in the global and regional functions between healthy, HHD and HCM groups. Some patients showed distinct functional characteristics despite being diagnosed with the same cardiac disease, which led to further division into two clinically distinct subgroups based on echocardiographic findings. The HHD patients were divided into HHD with preserved ejection fraction (HHDpEF) and reduced ejection fraction (HHDrEF). The HHDpEF group was identified as the ones with echocardiography measured EF≥50% while the HHDrEF group had reduced EF of <50% (Marwick, 2015). The HCM were also split into two groups with left ventricular outlet

obstruction (HOCM) and without left ventricular outlet obstruction (HNOCM). From echocardiograms, the HOCM group showed elevated resting pressure gradient across LVOT of >30mmHg while the HNOCM had resting pressure gradient across LVOT ≤30mmHg (Kwon et al., 2008; M. S. Maron et al., 2003).

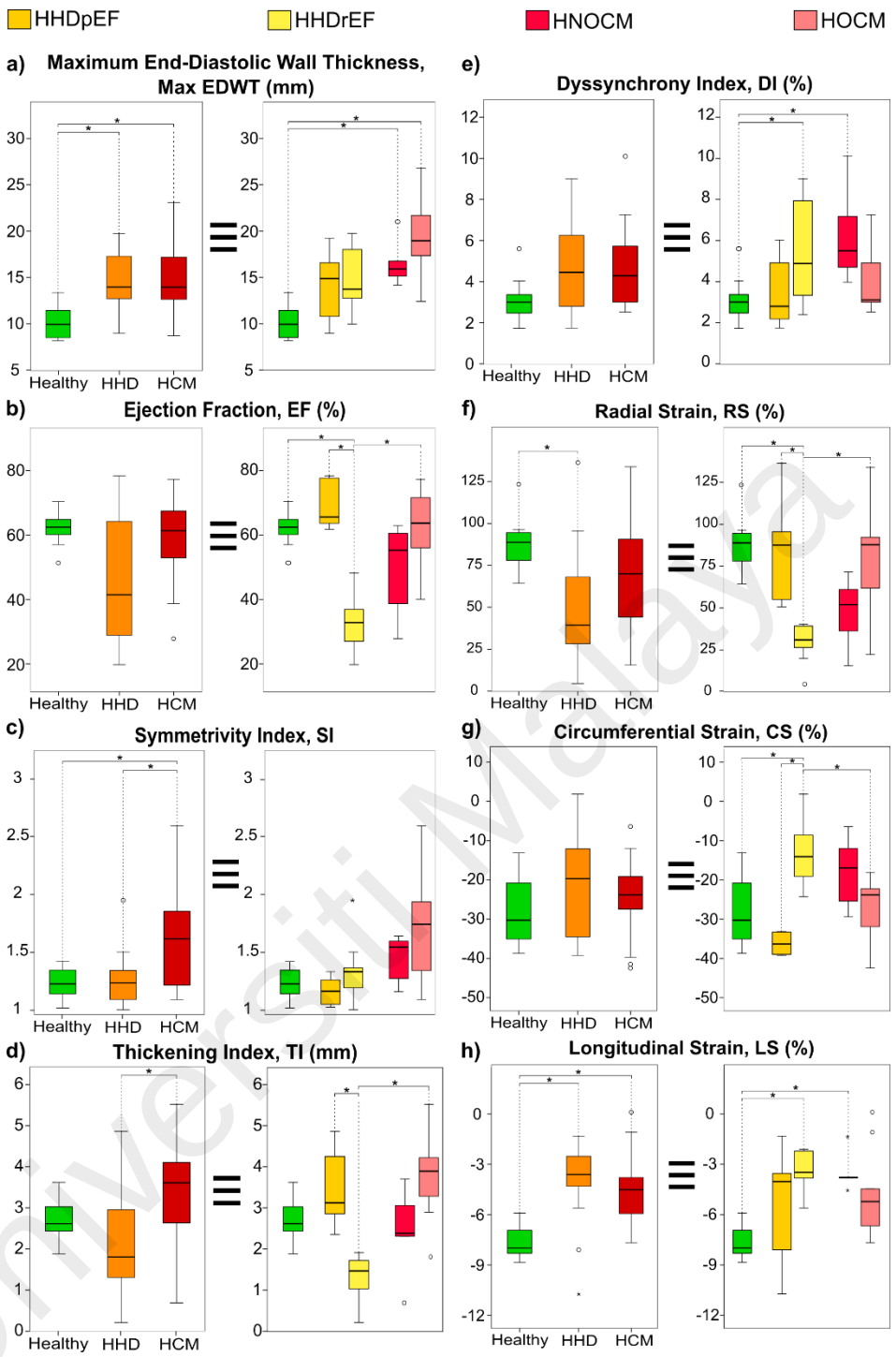

Figure 4.1: The LV functional parameters (a) Max EDWT, b) EF, c) TI, d) SI, e) DI, f) RS, g) CS and h) LS for the 3-group (healthy, HHD and HCM) and 5-group (healthy, HHDpEF, HHDrEF, HNOCM and HOCM) comparisons. (Note: *represents the significant difference between the compared groups whereby p-value <0.05).

Consistent with clinical findings, in 3-groups comparison as shown in Figure 4.1(a), HCM and HHD patients had significantly hypertrophied LV wall as compared with healthy subjects, as reflected by max EDWT of 17.6(4.3)mm and 14.0(4.2)mm respectively versus 9.9(2.6)mm. In 5-groups comparison, significant difference was found for the max EDWT between HNOCM and HOCM subgroups. The thicker myocardial wall is reflected by the LV mass (Table 4.1), as the average mass matches the increase in max EDWT, with HCM having the greatest LV mass (190.1(70.3)g), followed by HHD patients (167.6(50.5)g) and healthy subjects (82.8(15.6)g).

HCM patients maintained EF close to normal range, whereas HHD patients exhibited lower EF with a large interquartile range (Figure 4.1(b)). Using subgrouping, 62.5% of the HHD patients (i.e. HHDrEF) had severely reduced EF of 32.8(9.5)%, the lowest amongst all other groups and subgroups, whereas the other 37.5% (i.e. HHDpEF) exhibited normal or supernormal EF under the influence of high blood pressure. In addition, the HNOCM subgroup had significantly lower EF of 55.2(21.9)% in comparison to the HOCM subgroup that seemed to maintain EF within normal range. In Figure 4.1(c), HCM patients are also characterized by asymmetrical hypertrophy with higher score of SI (1.6(0.6)) than healthy group (1.2(0.2)) and HHD (1.2(0.2)). The higher SI score visually appears to be contributed mostly by the HCM group as compared with healthy and HHD in the 3-group comparison; however, no significant difference was observed in the SI score between the HCM subgroups.

In terms of TI and DI, HHDpEF and HOCM show greater wall thickening (higher TI value) when comparing between their own subgroups and normal wall synchrony (lower DI value) during systole as compared to healthy subjects, therefore yielding supernormal EF. Conversely, the deterioration of wall thickening coupled with dyssynchrony in wall

contractility of HHDrEF patients served to attenuate the EF. For HNOCM patients, they seemed to maintain normal wall thickening but worse wall synchrony, resulting in overall reduction in EF. Reduction in EF was also noted to associate with attenuation of myocardial strain. Whilst LS was significantly reduced in all patient groups, significant decline in RS and CS were primarily seen in HHDrEF due to impaired LV dynamic mechanism (i.e. RS: HHDrEF (31.0(11.0)%) vs healthy (88.8(15.3)%); CS: HHDrEF (-14.1(9.2)%) vs healthy (-30.3(13.7)%)). No significant difference was observed in the RS and CS of HHDpEF and HCM subgroups as compared to healthy group.

4.2 Case Studies on 3D Personalized Modeling to Aid Qualitative and Quantitative Assessment of HCM and HHD

The color-map 3D LV models illustrated information about myocardial thickening among healthy, HHD and HCM population. Figure 4.2 depicts the LV wall thickness between healthy, HHD and HCM patients relative to the cardiac cycle which involved both the ES and ED phases. Healthy LV models revealed a more consistent and uniform cardiac movement (contraction and relaxation) compared with HHD and HCM. Significant differences were observed through the LV models especially during the ED phase, indicating heterogeneous LV functions resulting from unusual myocardial thickening on HHD and HCM patients. The hypertrophied regions were represented through the alteration of the color from minor wall thickening to severe hypertrophy as displayed by the color bar (from cool colors to warm colors). For HHD and HCM, both LV models had larger potions of hypertrophied regions (orange-to-red color) throughout the cardiac phases. HHD LV models showed a greater extent of LV hypertrophy than healthy subjects with wall thickness approximately 15mm at ED phase. However, HCM patients had even thicker LV wall and wider affected area than HHD and healthy subjects. About 70% of the HCM LV models displayed orange and dark red colors due to

hypertrophic wall with wall thickness ranging roughly from 15 mm to 20 mm at ED phase. Hence, a segmental analysis of the EDWT were computed to allow further insight into the differences of the spatial wall thickness on these three different groups.

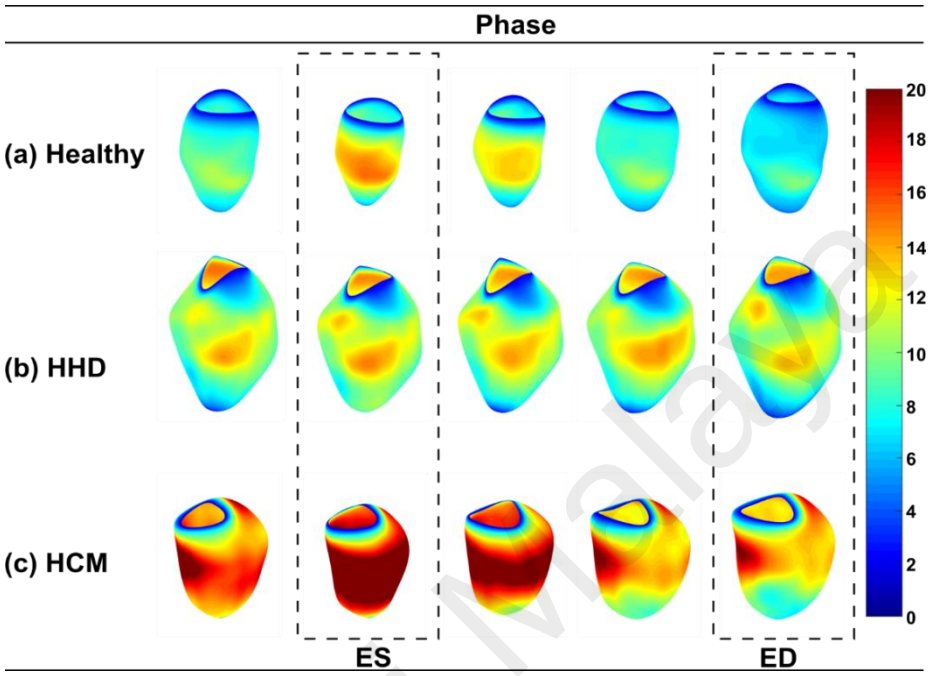

Figure 4.2: Three-dimensional personalized LV models color-coded with wall thickness measurements from individual healthy, HHD and HCM subjects at 5 selected cardiac phases. The size of the models is plotted to scale and wall thickness is represented by the color bar in mm. ES = End-Systole; ED = End-Diastole.

Figure 4.3 compares the bullseye diagrams of EDWT, AWT, time-to-peak and CS for five representatives of healthy, HHD and HCM patients, stratified by different degrees of severity based on the number of hypertrophied segments. Both moderate and severe HHD cases are from HHDrEF subgroups, whereas moderate and severe HCM cases are from HNOCM and HOCM subgroups, respectively. Comparing the HCM patients, the hypertrophied area in severe HCM was asymmetrically distributed with higher severity at septal segments, whilst hypertrophy was seen in basal- and mid-anteroseptal, -anterior and -anterolateral segments in moderate HCM. The severe HCM patient was diagnosed with LVOT obstruction, consistent with the observation of thickened wall along almost the entire basal circumference. On the other hand, more symmetrical and less severe

hypertrophy (9-15mm) was observed in HHD groups, although minor localized hypertrophy was noticeable from case to case. Degree of severity was also directly reflected by the escalation of LV mass from healthy (78.5g), moderate HHD (134.6g), severe HHD (182.5g), moderate HCM (187.5g) to severe HCM (490.8g) cases.

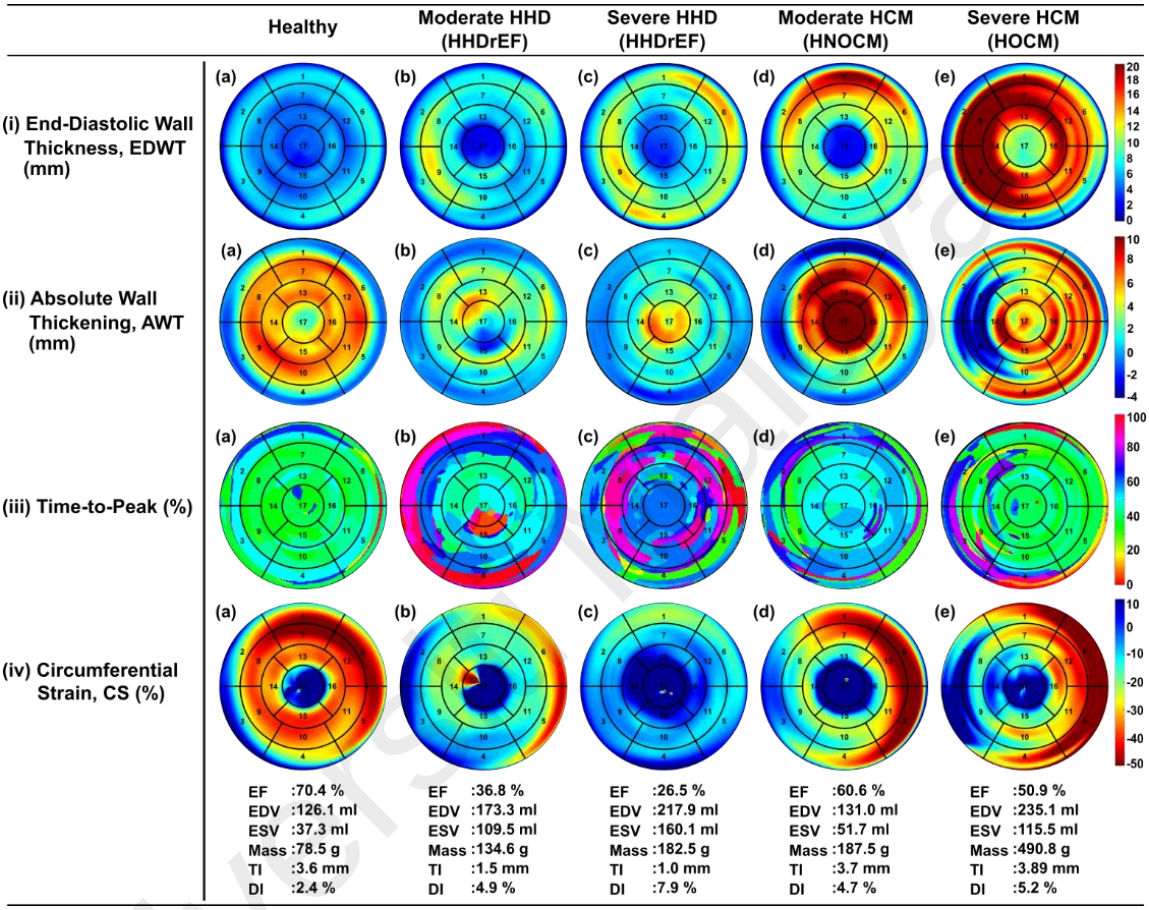

Figure 4.3: Bullseye diagrams for EDWT, AWT, time-to-peak, and circumferential strain for healthy, HHD and HCM patients, graded in terms of severity. Note: the color of circumferential strain is presented consistently with AWT, whereby red color implies high circumferential shortening and wall thickening respectively. Radial strain is omitted due to similarity to AWT.

For cardiac dynamics in terms of AWT, Figure 4.3(ii) illustrates that healthy LV could thicken by 6.1±1.3mm predominantly at mid and apical segments from ED to ES (with TI of 3.6mm), and less thickening occurred at the basal region towards the opening of the inflow and outflow tracts to allow unobstructed flow of blood. The LV of healthy subject also exhibited uniform contraction at all segments, achieving maximum thickening at

~40% of the R-R interval (as portrayed by green-to-cyan color across majority of the surface area in the time-to-peak plot (Figure 4.3(iii)(a)) and low DI value of 2.4%). Aside from that, circumferential shortening occurs and covers a wide area from basal to apical sections, excluding the apex (Figure 4.3(iv)). In contrast, AWT for moderate and severe HHDrEF patients were very low at 2.5±0.7mm and 1.6±0.9mm, respectively, consistent with their low TI values (Figure 4.3(ii)(b)&(c)). The time-to-peak plots of both HHDrEF patients appear chaotic with all cardiac segments contracting out-of-synch (i.e. as seen from the abrupt changes of color in Figure 4.3(iii)(b)&(c) with high DI value of 4.9-7.9%). CS was also low in both patients (Figure 4.3(iv)(b)&(c)). Co-occurrence of low AWT, attenuation of CS and higher DI is believed to contribute to reduce EF (26-37%) in these patients as compared to healthy subjects (~60-70%).

Despite severe wall hypertrophy, strong AWT and CS values were observed in HCM patients as opposed to HHD patients, which may help to maintain the EF at a normal range. This preserved EF was observed to be regulated by hypercontraction/normocontraction of the less/non-hypertrophic region (e.g. segment 17 in dark red in Figure 4.3(ii)(d)) and better coordinated contraction of all segments (i.e. less drastic change of color in the time-to-peak plot in Figure 4.3(iii)(d)&(e)) as compared to HHD patients. Although EF is normal, localized functional defects were observed, whereby the extremely hypertrophic region (septal wall) of severe HCM patients underwent wall thinning and reduction in CS during systole. Upon further investigation of LGE scans, the hypertrophic region of this particular patient was loaded with diffused fibrosis (Figure 4.4) leading to myocardial stiffness and loss of contractility (Gradman & Alfayoumi, 2006). This wall thinning is believed to be due to pulling and stretching by healthy functional surrounding myocardium during transition from diastole to systole (Y. M. Liew et al., 2018).

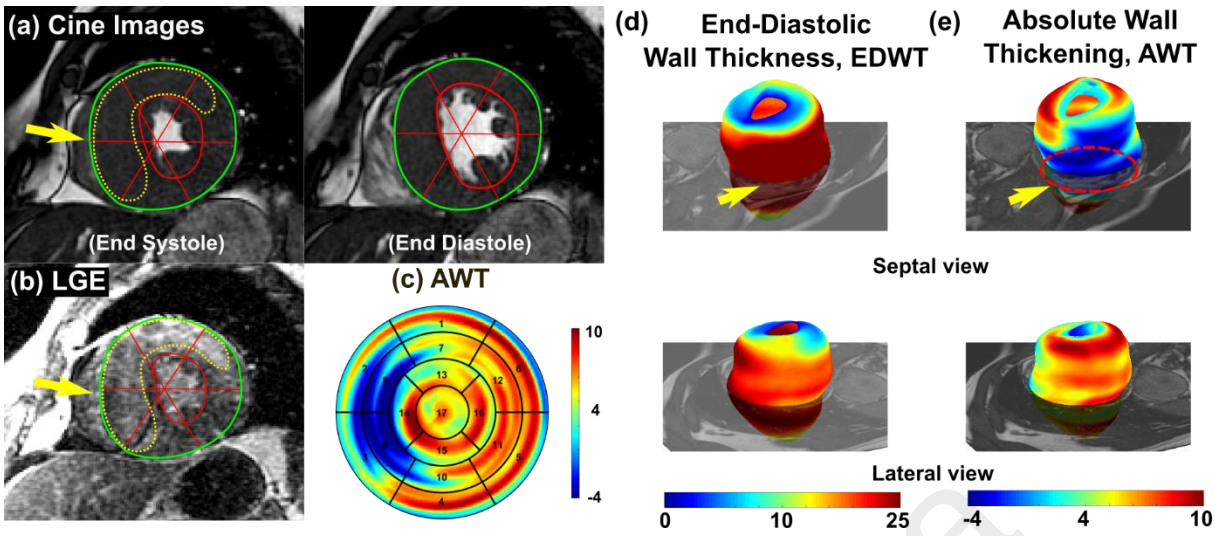

Figure 4.4: Correlation of the presence of fibrosis with low AWT. (a) shows the cine images with the endo- and epicardial contour as well as fibrosis, respectively in red, green and yellow outlines, at ES and ED phases. The same outlines were overlaid on top of the LGE image in (b). (c) shows the bullseye map of AWT. (d) shows the EDWT, whereas (e) shows the corresponding AWT in both in septal and lateral views, respectively. Fibrosis is affecting mainly the septal and anterior wall, which corresponds to the dark blue area within red dash-dotted line ellipse in (e) whereby thinning occurs from ED to ES. Colorbar indicates measurements in mm.

Figure 4.5 illustrates an overall segmental analysis of all patients to allow further insight into the difference in the distribution of max EDWT between the three groups. All segments were stratified into one of the three categories: EDWT≤9mm (presented by yellow color), 9mm<EDWT<15mm (presented by orange color), and EDWT≥15mm (presented by red color). Each segment was colored based on the majority vote of the category and the number within each segment indicates the percentage of patients that falls within the category. In healthy subjects, nearly all segments had max EDWT≤9mm except for the basal-inferoseptal segment that fall within the categories of EDWT between 9mm to 15mm (colored in orange). Whilst for HHD patients, majority of the segments (i.e. 13/17 segments) had higher max EDWT predominantly in 9mm<max EDWT<15mm category. The hypertrophy was spotted at the basal, mid and apical inferior segments, while the remaining segments (mainly the apical segments) had normal max EDWT≤9mm. In contrast, HCM patients showed higher probability of extreme

hypertrophy (max EDWT≥15mm) at the basal-anteroseptal, basal-inferoseptal, mid-anteroseptal, mid-inferoseptal and basal-anterolateral segments with 56-70% of the patients affected at these regions. Whilst, 10/17 of the segments in HCM patients had max EDWT in between 9mm and 15mm, whereas normal max EDWT≤9mm was observed at the apical lateral and apex regions.

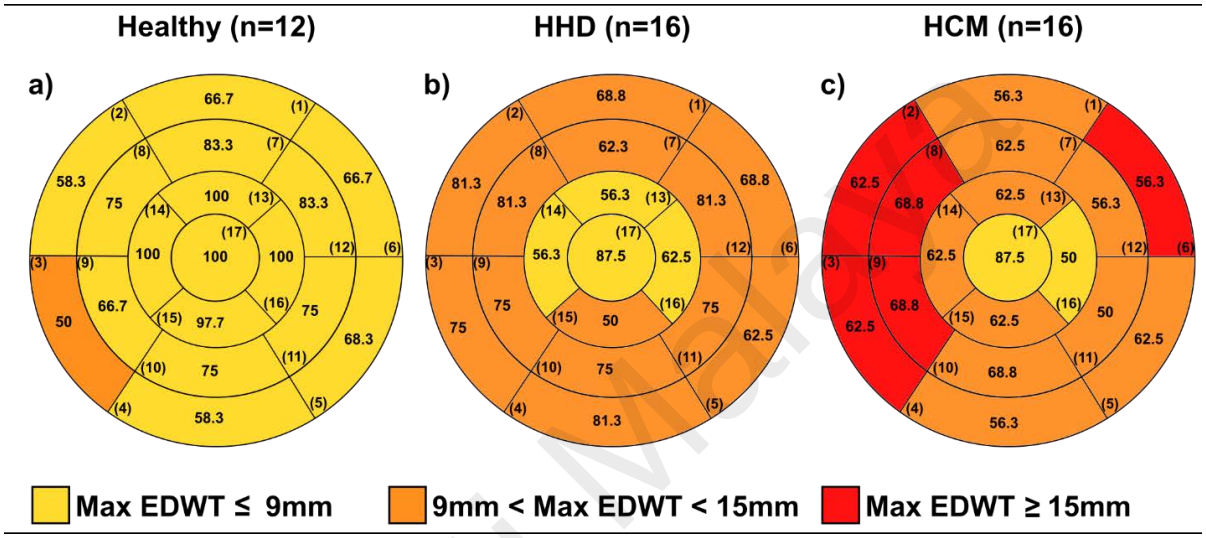

Figure 4.5: Stratification of spatial wall thickness based on segmental max EDWT for healthy, HHD and HCM patients. Each segment is color-coded with a specific EDWT category based on majority vote and the number (middle) represent the percentage of patients. The segment number is indicated by the labels in bracket.

4.3 Classification and Determination of Biomarkers for Predicting Healthy, HHD and HCM Cases

Table 4.2 shows the classification performance of various sets of data as tested by different classifiers. The 3 main groups – healthy, HHD and HCM – were classified with the highest performance by Support Vector Machine (sequential minimal optimization) Classifier (Accuracy: 0.77; FN Rate: 0.12; Precision: 0.79; F-Measure: 0.77; MCC: 0.66; ROC Area: 0.84; PRC Area: 0.71). Nevertheless, the level of performance is considered moderate indicating overlapping LV features among these three main groups. Therefore, further analysis was carried out to evaluate this hypothesis through selective removal of

patients' subgroups before classification. The highest classification accuracy was achieved with SVM (SMO), LR and NN(MLP) when only healthy, HHDrEF and HOCM patients were classified (Accuracy: 0.94; FN Rate: 0.03; Precision: 0.94-0.95; F-Measure: 0.94; MCC: 0.91-0.92; ROC Area: 0.97-0.99; PRC Area: 0.92-0.99). This indicated overlapping functional features, stemming from misclassifying some HHDpEF cases as healthy and HOCM, along with misclassifying some HNOCM cases as HHDrEF.

Table 4.2: Performance of different classifiers in differentiating healthy, HHD and HCM patients. HHD consists of HHDrEF and HHDpEF, whereas HCM consists of HNOCM and HOCM.

Grouping	Classifier	Accuracy	FP Rate	Precision	F-Measure	MCC	ROC Area	PRC Area
Healthy (n=12) + HHD (n=16) + HCM (n=16)	RF	0.66	0.18	0.65	0.65	0.48	0.83	0.73
	SVM (SMO)	0.77	0.12	0.79	0.77	0.66	0.84	0.71
	NB	0.71	0.16	0.71	0.70	0.55	0.84	0.77
	LR	0.66	0.18	0.66	0.66	0.48	0.86	0.74
	NN (MLP)	0.71	0.14	0.71	0.69	0.56	0.88	0.84
Healthy (n=12) + HHDrEF (n=10) + HCM (n=16)	RF	0.74	0.08	0.70	0.72	0.64	0.87	0.71
	SVM (SMO)	0.79	0.08	0.71	0.75	0.69	0.88	0.71
	NB	0.71	0.09	0.73	0.72	0.63	0.90	0.77
	LR	0.50	0.13	0.60	0.54	0.40	0.84	0.71
	NN (MLP)	0.76	0.07	0.72	0.74	0.68	0.87	0.75
Healthy (n=12) + HHD (n=16) + HOCM (n=11)	RF	0.77	0.08	0.74	0.74	0.68	0.92	0.80
	SVM (SMO)	0.85	0.06	0.85	0.84	0.80	0.94	0.81
	NB	0.74	0.10	0.85	0.73	0.65	0.94	0.84
	LR	0.67	0.12	0.69	0.66	0.56	0.89	0.78
	NN (MLP)	0.82	0.06	0.83	0.82	0.77	0.98	0.94
Healthy (n=12) + HHDrEF (n=10) + HOCM (n=11)	RF	0.88	0.06	0.88	0.88	0.82	0.96	0.93
	SVM (SMO)	0.94	0.03	0.95	0.94	0.92	0.97	0.92
	NB	0.85	0.08	0.85	0.85	0.77	0.97	0.96
	LR	0.94	0.03	0.95	0.94	0.92	0.99	0.99
	NN (MLP)	0.94	0.03	0.94	0.94	0.91	0.99	0.99

RF, Random Forest; SVM (SMO), Support vector machine (sequential minimal optimization); NB, Naïve Bayes; LR, Logistic Regression; NN (MLP), Neural network (multilayer perceptron); FP, False Positive; MCC, Matthews Correlation Coefficient; ROC, Receiver Operating Characteristic; PRC, Precision-recall curve (Note: The highlighted values represented the highest performance achieved by comparing all classifiers.)

Table 4.3 lists the top 5 LV functional parameters selected as significant features by multiple algorithms for differential diagnosis of healthy, HHD and HCM cases. The most frequently selected features by the algorithms were the maximum EDWT with a score of

5/5 chosen by the algorithms, followed by LS and M/V with score of 4/5, and the SI and mass with 3/5.

Table 4.3: Features selection by Correlation Feature Selection (CFS), correlation, information gain, gain ratio and reliefF methods for classification of healthy, HHD and HCM patients.

CFS	Correlation	Information Gain	Gain Ratio	ReliefF
Mass	Max EDWT	LS	Max EDWT	Fibrosis
Max EDWT	LS	Max EDWT	LS	Max EDWT
SV	SI	M/V	M/V	M/V
TI	M/V	Mass	Mass	LS
SI	Fibrosis	SI	SV	TI

Score	
Max EDWT	: 5/5
LS	: 4/5
M/V	: 4/5
SI	: 3/5
Mass	: 3/5

Max EDWT, maximum end-diastolic wall thickness SV, stroke volume; RS, radial strain; LS, longitudinal strain; SI, symmetricity index; M/V, mass-to-volume ratio.

To investigate how well the statistical model can be used to classify new incoming patients, we have selected SVM(SMO) and then used ten-fold cross validation to build a confusion matrix and calculated the positive predictive value (PPV aka precision), negative predictive value (NPV), sensitivity (aka recall) and specificity. Table 4.4 illustrates the confusion matrix for the classification of the 3 main groups (healthy, HHD and HCM) based on CMR phenotype data. We can see that the probability that subjects with a positive HCM diagnosis by SVM (SMO) truly have HCM is 90.9% (PPV), whereas the probability that subjects with a negative diagnosis truly do not have HCM is 81.8% (NPV). For HHD, the PPV and NPV are 66.7% and 84.6%, respectively (in comparison to 80% and 100% for healthy subjects).

Table 4.4: The confusion matrix for the classification of healthy, HHD and HCM cases by SVM(SMO).

		Predicted Class			
		Healthy	**HHD**	**HCM**	**Sens; Spec (%)**
Actual Class	**Healthy (12)**	12	0	0	100; 90.6
	HHD (16)	3	12	1	75; 78.6
	HCM (16)	0	6	10	62.5; 96.4
	PPV; NPV (%)	80; 100	66.7; 84.6	90.9; 81.8	

PPV, positive predictive value (aka precision); NPV, negative predictive value; Sens, Sensitivity (aka recall); Spec, specificity

The low PPV value for HHD and low sensitivity value for HCM was found to be due to the presence of HHDpEF and HNOCM subgroups. Our analysis (not shown) found when the classifier was made to differentiate all five classes, some HHDpEF cases were misclassified as healthy and HOCM cases, whereas some HNOCM cases were misclassified as HHDrEF and healthy cases. This assertion was confirmed by selective removal of HHDpEF and HNOCM cases from the training/building of the model, which resulted in significant improvement of the PPV, NPV, sensitivity and specificity values to 83% -100%. This is reflected in the following confusion matrix (TABLE 5), which implies that the CMR features tested were quite distinct between healthy, HHDrEF and HOCM groups when the 2 ambiguous groups were removed.

Table 4.5: The confusion matrix for the classification of healthy, HHDrEF and HOCM cases by SVM (SMO).

		Predicted Class			
		Healthy	**HHDrEF**	**HOCM**	**Sens; Spec (%)**
Actual Class	**Healthy (12)**	11	1	0	91.7; 100
	HHDrEF (10)	0	10	0	100; 91.3
	HOCM (11)	0	1	10	90.9; 100
	PPV; NPV(%)	100; 95.5	83.3; 100	100; 95.6	

PPV, positive predictive value (aka precision); NPV, negative predictive value; Sens, Sensitivity (aka recall); Spec, specificity

CHAPTER 5: DISCUSSION

Different etiologies of LVH could be reflected in the phenotypical differences and discerned by means of multiparametric CMR imaging. Although thickened walls are usually more apparent in patients with HCM compared with HHD, a considerable overlap in LV geometry was noted in previous studies suggesting that it may be challenging to differentiate these diseases on the basis of static LV geometric features alone. In this research, the developed 3D+time personalized modeling technique provided localized segmental insight into cardiac geometry and deformation, producing additional information about the characteristics of HHD and HCM in both the spatial and temporal domain. This method is unaffected by errors stemming from longitudinal shortening and non-perpendicular slice-wall intersection during the assessment of regional parameters across phases such as wall thickening and strain assessment as in manual 2D analysis (Puntmann et al., 2010; Rodrigues et al., 2017; Sipola et al., 2011). In contrast to the previous studies, which targeted only mild-to-moderate severity (Sipola et al., 2011), EDWT≥15mm and non-LVOT obstruction cases (Rodrigues et al., 2017), this research included more variations in the patient pool to investigate the subgroups of patients and their overlapping CMRI characteristics that specifically cause difficulties in differential diagnosis between HHD and HCM. Specifically, the HHD patients in this research included those with mild and severe symptoms (i.e. preserved and reduced EF), whereas the HCM patients included those with and without LVOT obstruction.

The 3D regional measurements (EDWT, AWT, time-to-peak and CS) were mapped onto bullseye diagrams to distinguish the hypertrophic sites and contraction patterns between HHD and HCM patients in relation to fibrosis. Greater max EDWT and focal/asymmetrical hypertrophy were determined predominantly at septal and antero-

lateral segments in majority of the HCM patients, whereas more globalized and homogeneous hypertrophy were displayed by HHD patients, which is in line with prior studies (Kuroda, Kato, & Amano, 2015; Urbano-Moral et al., 2013). Fibrosis was found in 62.5% (or 10/16) HCM and only 6.25% (1/16) HHD patients, consistent with Sipola et al. (2011) that LGE occurs in most of the HCM patients (up to 80% in their study) and Rudolph et al. (2009) who reported that patients with arterial hypertension may show the presence of LGE. In this research, it is noted that when the hypertrophy was too extreme (i.e. >26mm in 2 HCM patients) and affected by fibrosis, the LV wall ceased to contract resulting in wall thinning rather than thickening during systole. Myocardial fibrosis was suggested to initiate ventricular rigidity (increased wall stiffness), which reduces regional LV functions such as the myocardial strain/thickening (Y. M. Liew et al., 2018). The wall thinning was believed to be due to the pulling and stretching by the surrounding healthy tissue contracting during systole (Urbano-Moral et al., 2013).

The distortion of LV contraction and relaxation affects the filling and ejection of the blood volume. This research demonstrated that for HCM patients having severe focal hypertrophy, wall thickening was maintained and occasionally exaggerated at less severe hypertrophic regions during systole, resulting in overall preserved EF. This was previously categorized as extremely hypertrophied myocardial-induced hyperejected status affecting mostly early-stage HCM patients (Xu et al., 2017), whereby EF values appear preserved or higher than normal, while diastolic function seem deteriorated. As for HHD patients, 62.5% were found to have significantly reduced EF (HHDrEF) while the remaining had EF within normal range (HHDpEF). Such a reduction in EF is believed to be an indicator of systolic heart failure, often observed among hypertensive patients with adverse remodeling leading to heart dilation (Gradman & Alfayoumi, 2006; Shirwany & Weber, 2006) and this is supported by larger EDV for HHDrEF patients as

observed in this study. In contrast, though with preserved EF, the HHDpEF patients had significantly higher M/V ratio than normal, and could potentially succumb to diastolic heart failure as previously reported (Chatterjee & Massie, 2007).

Previously, Rodrigues et al. (2016) found that HHD patients showed reduced myocardial strain regardless of preserved EF. This research shows the contrary whereby HHDpEF patients have completely normal cardiac dynamics despite wall hypertrophy (Table 5.1), whereas only HHDrEF patients have deterioration in all cardiac dynamic values (including TI, DI and all strain indices) which contributed to lower EF. The difference is suspected due to Rodrigues' selection of HHD patients with extreme hypertrophy (wall thickness ≥ 15mm) and the use of 2D analysis. The reduction of EF in HHDrEF patients is most likely an indication of remodeling of the LV towards heart failure with cavity dilation (HHDrEF patients had EDV of 214.4(77.0)ml versus healthy 125.3(10.3)ml). For HCM patients, contractility impairment as in longitudinal shortening was suggested due to myocardial disarray that deteriorates the principal systolic shortening, torsional systolic shear and sarcomere shortening (Ennis et al., 2003; Yang et al., 2003). The impairment, however, was somehow compensated by either normal or supernormal contraction in the radial and/or circumferential directions leading to preserved EF in these patients, especially in HOCM.

Table 5.1: Deviation of cardiac structures, functions and dynamics of patients against normal. The increment of EDWT was identified by comparing to the healthy cohorts which has Max EDWT of 9.9 (2.6) mm.

Group	Subgroups	Max EDWT (Median(IQR))	Fibrosis	EF	TI	DI	RS	CS	LS
HHD (n=16)	HHDpEF (n=6)	↑ (14.9 (5.0))	0/6	N	N	N	N	N	N
	HHDrEF (n=10)	↑ (13.7 (4.4))	1/10	↓	↓	↑	↓	↓	↓
HCM (n=16)	HNOCM (n=5)	↑ (15.9 (1.6))	2/5	N	N	↑	↓	N	↓
	HOCM (n=11)	↑ (19.0 (4.4))	8/11	N	↑	N	N	N	↓

* N- normal; ↓ - reduce; ↑- increase

From the classification results, differentiating patients into 3 groups, i.e. healthy, HHD and HCM yielded moderate classification accuracy (≈66%-77%) and the top 5 significant features for classification included maximum EDWT, LS, M/V, SI and mass. Highest accuracy achievable is 99% when only classifying healthy, HHDrEF and HOCM patients (i.e. by selectively removing HHDpEF and HNOCM patients). This additional experiment provides insight that HHDpEF and HNOCM patients were mostly misdiagnosed into other groups due to the "grey area of overlap" in features, explaining the challenge in diagnosing these patients correctly. This is the first study to identify the subgroups of patients and their characteristics that often lead to ambiguity in differential diagnosis between HHD and HCM, with the aim to potentially steer future research in discovering novel useful biomarkers for improved diagnosis of these patients.

One limitation to this research is the relatively small number of subjects used; this therefore warrants testing in larger populations to derive solid conclusions on any clinical findings. Secondly, manual correction of LV contours is still required despite the use of the in-house automated LV segmentation algorithm based convolution neural network regression for SA scans (Tan et al., 2017; Tan et al., 2018). This was mainly due to the lack of HHD and HCM cases in the training sets in the building of the automated

segmentation framework. The incorporation of these cases for training as well as the extension of the algorithm for LA images can be foreseen to bring time efficiency for clinical diagnosis, subject to regular inspection of the accuracy especially on special cases with unique LV. Nevertheless, this study provides the first multiparametric assessment using 3D+time LV modeling techniques for visualization, quantification and differential diagnosis of HHD and HCM cases. Such technique allows full utilization of all cine scans for assessing LV functions which is currently infeasible using clinical 2D manual method. Both static and dynamics LV functional parameters can be extracted automatically using the proposed approach. In addition, the proposed method provides a visual aid which may be used to assess treatment efficacy, e.g. possible regression of LVH can be re-examined after the patient has been normotensive for several months under anti-hypertensive treatment (Marwick et al., 2015).

CHAPTER 6: CONCLUSION AND FUTURE WORK

6.1 Conclusion

In this study, an in-house 3D+time personalized LV modeling technique was evaluated to compare the geometry, functions and dynamics of HHD and HCM patients against healthy subjects. The proposed approach involves segmentation and reconstruction of LV models across full cardiac cycle from cine MRI to phenotype the LV of individual patients. This approach together with the 17 segments bullseye diagram for spatial mapping of regional metrics could improve the assessment of localized abnormalities of LV. The findings indicate the presence of distinctive phenotypes detectable by means of multiparametric MRI although there exist subgroups of patients with overlapping features that could potentially be researched in the future for improved diagnosis. Overall, LV systolic function is impaired with reduced TI, increased DI, and the attenuation of myocardial strain measurements, which correlates with severity of hypertrophy. Integrating both global and regional measurements as in this research was found useful and innovative measures may be explored in future research for discriminating HHD and HCM patients with higher confidence. The improved capability to differentiate and diagnose the etiology of LVH particularly at an early stage will help in better planning and execution of patients' short and long-term management strategies.

6.2 Suggestions for Future Work

The results of current study show that 3D personalized LV models using cine MRI could provide comprehensive and promising measurements in the diagnosis of patients with HHD and HCM. Suggestions in upgrading the present methodology for future work are discussed in the following subsections.

6.2.1 Larger Datasets with Various LVH Phenotypes

Present study used a total of 44 subjects which included 12 healthy subjects, 16 HHD patients and 16 HCM patients. A larger number of multicenter datasets is required in the future to validate the present 3D modeling framework. Furthermore, various LVH phenotypes (such as aortic stenosis, Fabry disease, sarcoidosis and amyloidosis) are recommended to be included to expand the database and to determine specific and significant LV features that are useful for their differentiation. The incorporation of these phenotypes will allow current techniques to explore potential prognostic factor for clinical diagnosis.

6.2.2 Fully Automated Image Segmentation

In the present study, the 3D motion corrected LV reconstruction algorithm and the wall thickness extraction methods are fully automatic but the segmentation of MRI images remains semi-automated. A readily build computed software (Segment) was utilized in this study to segment the MRI cine images semi-automatically. This application software is convenient to accurately delineate the borderline of epi- and endo-cardial wall in both SA and LA MRI cine images. Although manual delineation of epi- and endo-cardial wall is not hard to perform, it is still quite time consuming to complete the segmentation of each patient and is subject to observer variation. Hence, a fully automated image segmentation method is proposed for future work. Additionally, a more advanced border and pattern recognition algorithm is suggested to integrate with the semi-automated segmentation algorithm to improve the accuracy and precision of segmentation. With huge datasets, a fully automated image segmentation technique is required to help in reducing the workload and time consumption in completing the reporting of MRI scans.

6.2.3 Application of Machine Learning Techniques for Segmental LV Features Analysis

For this study, machine learning techniques were utilized to classify healthy, HHD and HCM cases by using the LV features computed from the 3D LV models. Currently the input data consisted of the global (e.g. LV mass, EF, EDV, etc.) and the average value of the regional (e.g max EDWT, TI, DI, SI, myocardial strain) LV features. All segmental LV features may be input individually to the machine learning algorithm if the number of subjects is huge enough. Segmental LV features such as EDWT and myocardial strain from the 17 segments AHA models might shed some light in determining powerful prognostic factor of various cardiac diseases.

REFERENCES

Alfakih, K., Plein, S., Thiele, H., Jones, T., Ridgway, J. P., & Sivananthan, M. U. (2003). Normal human left and right ventricular dimensions for MRI as assessed by turbo gradient echo and steady ‐ state free precession imaging sequences. *Journal of Magnetic Resonance Imaging: An Official Journal of the International Society for Magnetic Resonance in Medicine, 17*(3), 323-329.

Alis, D., Guler, A., Yergin, M., & Asmakutlu, O. (2020). Assessment of ventricular tachyarrhythmia in patients with hypertrophic cardiomyopathy with machine learning-based texture analysis of late gadolinium enhancement cardiac MRI. *Diagnostic and Interventional Imaging, 101*(3), 137-146.

Alkema, M., Spitzer, E., Soliman, O. I., & Loewe, C. (2016). Multimodality imaging for left ventricular hypertrophy severity grading: a methodological review. *Journal of cardiovascular ultrasound, 24*(4), 257-267.

Amin, M. S., Chiam, Y. K., & Varathan, K. D. (2019). Identification of significant features and data mining techniques in predicting heart disease. *Telematics and Informatics, 36*, 82-93.

Ammirati, E., Contri, R., Coppini, R., Cecchi, F., Frigerio, M., & Olivotto, I. (2016). Pharmacological treatment of hypertrophic cardiomyopathy: current practice and novel perspectives. *European journal of heart failure, 18*(9), 1106-1118.

Ardekani, S., Jain, S., Sanzi, A., Corona-Villalobos, C. P., Abraham, T. P., Abraham, M. R., . . . Younes, L. (2016). Shape analysis of hypertrophic and hypertensive heart disease using MRI-based 3D surface models of left ventricular geometry. *Medical Image Analysis, 29*, 12-23. doi: https://doi.org/10.1016/j.media.2015.11.004

Authors/Task Force members, Elliott, P. M., Anastasakis, A., Borger, M. A., Borggrefe, M., Cecchi, F., . . . Limongelli, G. (2014). 2014 ESC Guidelines on diagnosis and management of hypertrophic cardiomyopathy: the Task Force for the Diagnosis and Management of Hypertrophic Cardiomyopathy of the European Society of Cardiology (ESC). *European Heart Journal, 35*(39), 2733-2779.

Beohar, N., Flaherty, J. D., Davidson, C. J., Vidovich, M. I., Brodsky, A., Lee, D. C., . . . Sheehan, F. H. (2007). Quantitative assessment of regional left ventricular function with cardiac MRI: Three ‐ dimensional centersurface method. *Catheterization and Cardiovascular Interventions, 69*(5), 721-728.

Berk, B. C., Fujiwara, K., & Lehoux, S. (2007). ECM remodeling in hypertensive heart disease. *The Journal of clinical investigation, 117*(3), 568-575.

Bhan, A., Sirker, A., Zhang, J., Protti, A., Catibog, N., Driver, W., . . . Shah, A. M. (2014). High-frequency speckle tracking echocardiography in the assessment of left ventricular function and remodeling after murine myocardial infarction. *American Journal of Physiology-Heart and Circulatory Physiology, 306*(9), H1371-H1383.

Bicudo, L. S., Tsutsui, J. M., Shiozaki, A., Rochitte, C. E., Arteaga, E., Mady, C., . . . Mathias Jr, W. (2008). Value of real time three‐dimensional echocardiography in patients with hypertrophic cardiomyopathy: comparison with two‐dimensional echocardiography and magnetic resonance imaging. *Echocardiography, 25*(7), 717-726.

Bruder, O., Wagner, A., Jensen, C. J., Schneider, S., Ong, P., Kispert, E.-M., . . . Sechtem, U. (2010). Myocardial scar visualized by cardiovascular magnetic resonance imaging predicts major adverse events in patients with hypertrophic cardiomyopathy. *Journal of the American College of Cardiology, 56*(11), 875-887.

Cerqueira, M. D., Weissman, N. J., Dilsizian, V., Jacobs, A. K., Kaul, S., Laskey, W. K., . . . Ryan, T. (2002). Standardized myocardial segmentation and nomenclature for tomographic imaging of the heart: a statement for healthcare professionals from the Cardiac Imaging Committee of the Council on Clinical Cardiology of the American Heart Association. *Circulation, 105*(4), 539-542.

Chatterjee, K., & Massie, B. (2007). Systolic and diastolic heart failure: differences and similarities. *Journal of cardiac failure, 13*(7), 569-576.

Chuang, M. L., Hibberd, M. G., Salton, C. J., Beaudin, R. A., Riley, M. F., Parker, R. A., . . . Manning, W. J. (2000). Importance of imaging method over imaging modality in noninvasive determination of left ventricular volumes and ejection fraction: assessment by two-and three-dimensional echocardiography and magnetic resonance imaging. *Journal of the American College of Cardiology, 35*(2), 477-484.

Chun, E. J., Choi, S. I., Jin, K. N., Kwag, H. J., Kim, Y. J., Choi, B. W., . . . Park, J. H. (2010). Hypertrophic cardiomyopathy: assessment with MR imaging and multidetector CT. *Radiographics, 30*(5), 1309-1328.

Corden, B., de Marvao, A., Dawes, T. J., Shi, W., Rueckert, D., Cook, S. A., & O'Regan, D. P. (2016). Relationship between body composition and left ventricular geometry using three dimensional cardiovascular magnetic resonance. *Journal of Cardiovascular Magnetic Resonance, 18*(1), 32.

de Marvao, A., Dawes, T. J., Shi, W., Minas, C., Keenan, N. G., Diamond, T., . . . Cook, S. A. (2014). Population-based studies of myocardial hypertrophy: high resolution cardiovascular magnetic resonance atlases improve statistical power. *Journal of Cardiovascular Magnetic Resonance, 16*(1), 16.

Ennis, D. B., Epstein, F. H., Kellman, P., Fananapazir, L., McVeigh, E. R., & Arai, A. E. (2003). Assessment of regional systolic and diastolic dysfunction in familial hypertrophic cardiomyopathy using MR tagging. *Magnetic Resonance in Medicine: An Official Journal of the International Society for Magnetic Resonance in Medicine, 50*(3), 638-642.

Frangi, A. F., Rueckert, D., Schnabel, J. A., & Niessen, W. J. (2002). Automatic construction of multiple-object three-dimensional statistical shape models:

Application to cardiac modeling. *IEEE transactions on medical imaging, 21*(9), 1151-1166.

Friedman, J. H., Bentley, J. L., & Finkel, R. A. (1977). An algorithm for finding best matches in logarithmic expected time. *ACM Transactions on Mathematical Software (TOMS), 3*(3), 209-226.

Gradman, A. H., & Alfayoumi, F. (2006). From left ventricular hypertrophy to congestive heart failure: management of hypertensive heart disease. *Progress in cardiovascular diseases, 48*(5), 326-341.

Heiberg, E., Sjögren, J., Ugander, M., Carlsson, M., Engblom, H., & Arheden, H. (2010). Design and validation of Segment-freely available software for cardiovascular image analysis. *BMC medical imaging, 10*(1), 1.

Johnson, C., Kuyt, K., Oxborough, D., & Stout, M. (2019). Practical tips and tricks in measuring strain, strain rate and twist for the left and right ventricles. *Echo research and practice, 6*(3), R87.

Kearney, P. M., Whelton, M., Reynolds, K., Muntner, P., Whelton, P. K., & He, J. (2005). Global burden of hypertension: analysis of worldwide data. *The lancet, 365*(9455), 217-223.

Kearney, P. M., Whelton, M., Reynolds, K., Whelton, P. K., & He, J. (2004). Worldwide prevalence of hypertension: a systematic review. *Journal of hypertension, 22*(1), 11-19.

Keller, H., Wanger, K. C., Goepfrich, M., Stegaru, B., Buss, J., & Heene, D. L. (1990). Morphological quantification and differentiation of left ventricular hypertrophy in hypertrophic cardiomyopathy and hypertensive heart disease A two dimensional echocardiographic study. *European Heart Journal, 11*(1), 65-74. doi: 10.1093/oxfordjournals.eurheartj.a059594

Khalid, A., Lim, E., Chan, B. T., Abdul Aziz, Y. F., Chee, K. H., Yap, H. J., & Liew, Y. M. (2019). Assessing regional left ventricular thickening dysfunction and dyssynchrony via personalized modeling and 3D wall thickness measurements for acute myocardial infarction. *Journal of Magnetic Resonance Imaging, 49*(4), 1006-1019.

Kreyszig, E. (2009). Advanced Engineering Mathematics, 10th Eddition: Wiley.

Kuroda, K., Kato, T. S., & Amano, A. (2015). Hypertensive cardiomyopathy: A clinical approach and literature review. *World Journal of Hypertension, 5*(2), 41-52.

Kwon, D. H., Setser, R. M., Thamilarasan, M., Popovic, Z., Smedira, N., Schoenhagen, P., . . . Desai, M. Y. (2008). Abnormal papillary muscle morphology is independently associated with increased left ventricular outflow tract obstruction in hypertrophic cardiomyopathy. *Heart, 94*(10), 1295-1301.

Lagarias, J. C., Reeds, J. A., Wright, M. H., & Wright, P. E. (1998). Convergence properties of the Nelder--Mead simplex method in low dimensions. *SIAM Journal on optimization, 9*(1), 112-147.

Leong, C. O., Lim, E., Tan, L. K., Abdul Aziz, Y. F., Sridhar, G. S., Socrates, D., . . . Liew, Y. M. (2019). Segmentation of left ventricle in late gadolinium enhanced MRI through 2D‐4D registration for infarct localization in 3D patient‐specific left ventricular model. *Magnetic resonance in medicine, 81*(2), 1385-1398.

LEVY, D., ANDERSON, K. M., SAVAGE, D. D., KANNEL, W. B., CHRISTIANSEN, J. C., & Castelli, W. P. (1988). Echocardiographically detected left ventricular hypertrophy: prevalence and risk factors: the Framingham Heart Study. *Annals of internal medicine, 108*(1), 7-13.

Liew, Y., McLaughlin, R., Chan, B., Aziz, Y. A., Chee, K., Ung, N., . . . Lim, E. (2015). Motion corrected LV quantification based on 3D modelling for improved functional assessment in cardiac MRI. *Physics in Medicine & Biology, 60*(7), 2715.

Liew, Y. M., Khalid, A., Tan, L. K., Lim, E., Chan, B. T., Sari, N. A. B. M., . . . Aziz, Y. F. A. (2018). *Spatial Cardiac Dysfunction Assessment via Personalized Modelling from MRI.* Paper presented at the 2018 IEEE-EMBS Conference on Biomedical Engineering and Sciences (IECBES).

Marian, A. J., & Braunwald, E. (2017). Hypertrophic cardiomyopathy: genetics, pathogenesis, clinical manifestations, diagnosis, and therapy. *Circulation research, 121*(7), 749-770.

Maron, B. J. (2002). Hypertrophic cardiomyopathy: a systematic review. *Jama, 287*(10), 1308-1320.

Maron, B. J. (2018). Clinical course and management of hypertrophic cardiomyopathy. *New England Journal of Medicine, 379*(7), 655-668.

Maron, B. J., Gardin, J. M., Flack, J. M., Gidding, S. S., Kurosaki, T. T., & Bild, D. E. (1995). Prevalence of hypertrophic cardiomyopathy in a general population of young adults: echocardiographic analysis of 4111 subjects in the CARDIA study. *Circulation, 92*(4), 785-789.

Maron, M. S., Olivotto, I., Betocchi, S., Casey, S. A., Lesser, J. R., Losi, M. A., . . . Maron, B. J. (2003). Effect of left ventricular outflow tract obstruction on clinical outcome in hypertrophic cardiomyopathy. *New England Journal of Medicine, 348*(4), 295-303.

Marwick, T. H., Gillebert, T. C., Aurigemma, G., Chirinos, J., Derumeaux, G., Galderisi, M., . . . Segers, P. (2015). Recommendations on the use of echocardiography in adult hypertension: a report from the European Association of Cardiovascular Imaging (EACVI) and the American Society of Echocardiography (ASE). *European Heart Journal-Cardiovascular Imaging, 16*(6), 577-605.

Noureldin, R. A., Liu, S., Nacif, M. S., Judge, D. P., Halushka, M. K., Abraham, T. P., . . . Bluemke, D. A. (2012). The diagnosis of hypertrophic cardiomyopathy by cardiovascular magnetic resonance. *Journal of Cardiovascular Magnetic Resonance, 14*(1), 17.

Pennell, D. J. (2002). Ventricular volume and mass by CMR. *Journal of Cardiovascular Magnetic Resonance, 4*(4), 507-513.

Pennell, D. J., Sechtem, U. P., Higgins, C. B., Manning, W. J., Pohost, G. M., Rademakers, F. E., . . . Kent Yucel, E. (2004). Clinical indications for cardiovascular magnetic resonance (CMR): Consensus Panel report. *Journal of Cardiovascular Magnetic Resonance, 6*(4), 727-765.

Popović, Z. B., Kwon, D. H., Mishra, M., Buakhamsri, A., Greenberg, N. L., Thamilarasan, M., . . . Desai, M. Y. (2008). Association between regional ventricular function and myocardial fibrosis in hypertrophic cardiomyopathy assessed by speckle tracking echocardiography and delayed hyperenhancement magnetic resonance imaging. *Journal of the American Society of Echocardiography, 21*(12), 1299-1305.

Prondzynski, M., Mearini, G., & Carrier, L. (2019). Gene therapy strategies in the treatment of hypertrophic cardiomyopathy. *Pflügers Archiv-European Journal of Physiology, 471*(5), 807-815.

Puntmann, V. O., Jahnke, C., Gebker, R., Schnackenburg, B., Fox, K. F., Fleck, E., & Paetsch, I. (2010). Usefulness of magnetic resonance imaging to distinguish hypertensive and hypertrophic cardiomyopathy. *The American journal of cardiology, 106*(7), 1016-1022.

Rodrigues, J. C., Rohan, S., Dastidar, A. G., Harries, I., Lawton, C. B., Ratcliffe, L. E., . . . Paton, J. F. (2017). Hypertensive heart disease versus hypertrophic cardiomyopathy: multi-parametric cardiovascular magnetic resonance discriminators when end-diastolic wall thickness⩾ 15 mm. *European radiology, 27*(3), 1125-1135.

Rodrigues, J. C., Rohan, S., Dastidar, A. G., Trickey, A., Szantho, G., Ratcliffe, L. E., . . . Hamilton, M. C. (2016). The relationship between left ventricular wall thickness, myocardial shortening, and ejection fraction in hypertensive heart disease: insights from cardiac magnetic resonance imaging. *The Journal of Clinical Hypertension, 18*(11), 1119-1127.

Rudolph, A., Abdel-Aty, H., Bohl, S., Boyé, P., Zagrosek, A., Dietz, R., & Schulz-Menger, J. (2009). Noninvasive detection of fibrosis applying contrast-enhanced cardiac magnetic resonance in different forms of left ventricular hypertrophy: relation to remodeling. *Journal of the American College of Cardiology, 53*(3), 284-291.

Sanaani, A., & Fuisz, A. (2019). Cardiac magnetic resonance for diagnosis and risk stratification. *Cardiology clinics, 37*(1), 27-33.

Semelka, R. C., Tomei, E., Wagner, S., Mayo, J., Kondo, C., Suzuki, J., . . . Higgins, C. B. (1990). Normal left ventricular dimensions and function: interstudy reproducibility of measurements with cine MR imaging. *Radiology, 174*(3), 763-768.

Sheehan, F. H., Bolson, E. L., Dodge, H. T., Mathey, D. G., Schofer, J., & Woo, H. (1986). Advantages and applications of the centerline method for characterizing regional ventricular function. *Circulation, 74*(2), 293-305.

Shirwany, A., & Weber, K. T. (2006). Extracellular matrix remodeling in hypertensive heart disease: Journal of the American College of Cardiology.

Sipola, P., Magga, J., Husso, M., Jääskeläinen, P., Peuhkurinen, K., & Kuusisto, J. (2011). Cardiac MRI assessed left ventricular hypertrophy in differentiating hypertensive heart disease from hypertrophic cardiomyopathy attributable to a sarcomeric gene mutation. *European radiology, 21*(7), 1383-1389.

Spartera, M., Damascelli, A., Mozes, F., De Cobelli, F., & La Canna, G. (2017). Three-dimensional speckle tracking longitudinal strain is related to myocardial fibrosis determined by late-gadolinium enhancement. *The international journal of cardiovascular imaging, 33*(9), 1351-1360.

Squeri, A., Censi, S., Reverberi, C., Gaibazzi, N., Baldelli, M., Binno, S. M., . . . Bosi, S. (2017). Three-dimensional echocardiography in various types of heart disease: a comparison study of magnetic resonance imaging and 64-slice computed tomography in a real-world population. *Journal of echocardiography, 15*(1), 18-26.

Sun, J. P., Xu, T. Y., Ni, X. D., Yang, X. S., Hu, J. L., Wang, S. C., . . . Wang, J. G. (2019). Echocardiographic strain in hypertrophic cardiomyopathy and hypertensive left ventricular hypertrophy. *Echocardiography, 36*(2), 257-265.

Swoboda, P. P., McDiarmid, A. K., Erhayiem, B., Law, G. R., Garg, P., Broadbent, D. A., . . . Foley, J. R. (2017). Effect of cellular and extracellular pathology assessed by T1 mapping on regional contractile function in hypertrophic cardiomyopathy. *Journal of Cardiovascular Magnetic Resonance, 19*(1), 16.

Tan, L. K., Liew, Y. M., Lim, E., & McLaughlin, R. A. (2017). Convolutional neural network regression for short-axis left ventricle segmentation in cardiac cine MR sequences. *Medical Image Analysis, 39*, 78-86.

Tan, L. K., McLaughlin, R. A., Lim, E., Abdul Aziz, Y. F., & Liew, Y. M. (2018). Fully automated segmentation of the left ventricle in cine cardiac MRI using neural network regression. *Journal of Magnetic Resonance Imaging, 48*(1), 140-152.

Tavakoli, V., & Amini, A. A. (2013). A survey of shaped-based registration and segmentation techniques for cardiac images. *Computer Vision and Image Understanding, 117*(9), 966-989.

Tobon-Gomez, C., Butakoff, C., Yushkevich, P., Huguet, M., & Frangi, A. (2010). *3D mesh based wall thickness measurement: identification of left ventricular hypertrophy phenotypes.* Paper presented at the Engineering in Medicine and Biology Society (EMBC), 2010 Annual International Conference of the IEEE.

Tsang, K., Chan, W., Shiu, C., Lee, J., & Chan, M. (2018). Magnetic Resonance Imaging of Hypertrophic Cardiomyopathy. *HONG KONG JOURNAL OF RADIOLOGY, 21*(4), 274-279.

Urbano-Moral, J. A., Rowin, E. J., Maron, M. S., Crean, A., & Pandian, N. G. (2013). Investigation of global and regional myocardial mechanics with 3-dimensional speckle tracking echocardiography and relations to hypertrophy and fibrosis in hypertrophic cardiomyopathy. *Circulation: Cardiovascular Imaging, 7*(1), 11-19.

van der Geest, R. J., de Roos, A., van der Wall, E. E., & Reiber, J. H. (1997). Quantitative analysis of cardiovascular MR images. *The International Journal of Cardiac Imaging, 13*(3), 247-258.

Whelton, P. K., He, J., Appel, L. J., Cutler, J. A., Havas, S., Kotchen, T. A., . . . Winston, M. C. (2002). Primary prevention of hypertension: clinical and public health advisory from The National High Blood Pressure Education Program. *Jama, 288*(15), 1882-1888.

Xu, H. y., Chen, J., Yang, Z. g., Li, R., Shi, K., Zhang, Q., . . . Guo, Y. k. (2017). Early marker of regional left ventricular deformation in patients with hypertrophic cardiomyopathy evaluated by MRI tissue tracking: The effects of myocardial hypertrophy and fibrosis. *Journal of Magnetic Resonance Imaging, 46*(5), 1368-1376.

Yang, H., Sun, J. P., Lever, H. M., Popovic, Z. B., Drinko, J. K., Greenberg, N. L., . . . Garcia, M. J. (2003). Use of strain imaging in detecting segmental dysfunction in patients with hypertrophic cardiomyopathy. *Journal of the American Society of Echocardiography, 16*(3), 233-239.

Zhao, L., Ma, X., Feuchtner, G. M., Zhang, C., & Fan, Z. (2014). Quantification of myocardial delayed enhancement and wall thickness in hypertrophic cardiomyopathy: multidetector computed tomography versus magnetic resonance imaging. *European journal of radiology, 83*(10), 1778-1785.

LIST OF PUBLICATIONS AND PAPERS PRESENTED

Journal Article

- Chuah SH, Sari NA, Chew BT, Tan LK, Chiam YK, Chan BT, Lim E, Aziz YF, Liew YM. Phenotyping of hypertensive heart disease and hypertrophic cardiomyopathy using personalized 3D modelling and cardiac cine MRI. Physica Medica. 2020 Oct 1;78:137-49.